Title

Interferon-β induction heterogeneity during KSHV infection is correlated to expression and activation of enhanceosome transcription factors other than IRF3

Authors

Machika Kaku[1,2] and Marta Maria Gaglia[2*]

[1]Program in Immunology, Tufts Graduate School of Biomedical Sciences, Boston, MA

[2]Department of Medical Microbiology and Immunology, Institute for Molecular Virology, and Carbone Cancer Center, University of Wisconsin - Madison, WI

ORCIDs: 0000-0002-9921-0678 (M.K.); 0000-0002-1791-0663 (M.M.G.)

[*]Correspondence and reprint requests to Dr. Marta Gaglia, University of Wisconsin-Madison, 1525 Linden Dr, Madison, WI 53706. E-mail address: marta.gaglia@wisc.edu. Phone number: (608)263-5551

Abstract

Careful regulation of type I interferons (IFN) is vital for balancing tissue damage and protection against infections. We previously found that during Kaposi's sarcoma-associated herpesvirus infection, type I IFN induction was limited to a small percentage of infected cells. This heterogeneity was not explained by viral gene expression. Here, we used a fluorescent reporter and fluorescence activated cell sorting to investigate the source of this heterogeneity. Surprisingly, the canonical IFN induction pathway culminating in the activation of the IRF3 transcription factor was similarly activated between cells that made high vs. low/no IFN-β. In contrast, the activation or expression of the two other IFN transcription factors, NF-κB and AP-1, correlated with IFN-β induction. Our results suggest that during viral infection, activation of IRF3 does not automatically result in IFN responses at the level of individual cells, but that other factors, such as NF-κB and AP-1, are limiting for type I IFN induction.

Importance

The ability of mammalian cells to react to viral infections is a crucial step in the induction of immune responses. The first course of action for the cell is to express and release type I interferons like interferon-β (IFN-β), secreted molecules that warn surrounding cells. Single-cell level examination of gene expression has revealed that surprisingly, during many viral infections, only a small fraction of infected cells makes IFN-β. This is likely a mechanism to prevent immune system overreactions. However, it remains unclear why only some cells respond. Here, we find that during infection with Kaposi's sarcoma-associated herpesvirus, an oncogenic virus that affects immunocompromised individuals, the transcription factors AP-1 and NF-κB, rather than the more commonly studied IRF3, may decide which cells go on to make IFN-β. Our findings contribute to a better understanding of complex gene regulation and shed light on a process that fights an oncogenic virus.

Introduction

Type I and III interferons (IFNs) such as interferon-β (IFN-β) and interferon-λs (IFN-λ) are potent cytokines that defend mammals against viral infections. As a key component of innate immunity, they are induced in response to pathogen-associated molecular patterns (PAMPs), such as nucleic acids with unfamiliar characteristics, or damage-associated molecular patterns (DAMPs) due to infection-induced stress. PAMPs and DAMPs are sensed by pattern recognition receptors (PRRs), leading to IFN induction. Type I and III IFNs then orchestrate antiviral defense by signaling through the IFNAR1/2 and IFNLR1/IL10Rβ receptor complexes, respectively, and induce hundreds of interferon stimulated genes (ISGs) (1). ISGs encode proteins that antagonize viral replication through a variety of mechanisms (2). Despite this crucial antiviral role, IFNs are well known to be a double-edged sword because of their powerful effects on cell and tissue physiology. While insufficient IFN signaling leaves the host susceptible to infections, excessive IFN signaling causes tissue damage and contributes to autoimmune disease development (3-5). Therefore, IFN-β and other type I and III IFNs are carefully regulated, and multiple host regulatory mechanisms have evolved to ensure their expression only under appropriate conditions.

An emerging dimension of IFN regulation is transcriptional heterogeneity at the single cell level. This aspect of IFN regulation has become clear from the growing number of single cell RNA sequencing (scRNA-seq) analyses of infected cells. We and others have found only a small percentage (<10%) of virus-infected cells produce IFN-β or IFN-λ (6-18). This has been reported in infections with the RNA viruses Influenza A Virus (7, 10, 11, 14-17), Newcastle Disease Virus (18, 19), West Nile Virus (13), and

SARS-CoV-2 (9), as well as the DNA viruses Herpes Simplex Virus 1 (12) and Human Cytomegalovirus (8), and in our studies in Kaposi's sarcoma-associated herpesvirus (KSHV) (6). We had previously discovered that KSHV hijacks the function of host caspases to prevent IFN-β induction when KSHV re-enters the replicative (lytic) cycle from a dormant (latent) infection state (20). Adding a small molecule caspase inhibitor restores activation of the cytoplasmic DNA-sensing PRR cyclic GMP-AMP synthase (cGAS) (6) and results in IFN-β induction (20). The amount of IFN-β produced under these conditions based on ELISA measurements was substantial (20). Nonetheless, subsequent scRNA-seq experiments revealed that the IFN-β comes from a small population of cells, with less than 4% of infected cells producing it even under this "derepressed" condition (6). The limited number of type I/III IFN producing cells across a range of infections and cell types indicate that this is a feature of the IFN induction system.

Since subversion of type I IFN is a key evolutionary tactic for viruses in the virus-host arms race, heterogeneity in the expression and activity of IFN-inhibiting viral proteins has been proposed as the reason for heterogeneous IFN-β expression (15, 20). However, we and others have found that viral gene expression heterogeneity does not fully explain the observed IFN-β heterogeneity during infection with a range of different viruses – KSHV, Influenza A Virus, Sendai Virus, and Newcastle Disease Virus (6, 11, 19, 21, 22). In our scRNA-seq experiments with KSHV, IFN-β was only detected in cells in the early stages of the KSHV lytic cycle, which made up 46% of the population, indeed suggesting a contribution from viral regulation of IFN (6). Cells that are latently infected with KSHV likely do not detect the infection, while cells in later lytic

viral stages have likely shut down host defenses. However, only 6% of the cells in the early lytic stages expressed IFN-β, demonstrating that viral replication stage does not completely determine IFN induction (6). Moreover, when we compared IFN-β positive and negative cells within this population, we did not find any viral gene that was specifically missing in IFN-β-producing cells, as would be expected for a heterogeneously expressed viral IFN suppressor (6). These findings suggested that there is an additional, likely cellular, source of IFN-induction heterogeneity in this system, which may explain the consistency of this phenomenon across viral infections. The host may benefit from limiting the percentage of cells producing IFN-β in an infected population, as this may allow for optimal distribution of the cytokine and protection of surrounding cells without IFNs reaching dangerous levels. However, how IFN induction is restricted to a few cells remains unclear.

A potential mechanism could be restricted activation of one of the many signaling steps that are needed for type I and III IFN transcriptional activation downstream of PRRs. While different PRRs rely on different signaling adaptors, their signaling pathways generally converge on the kinase TANK-binding kinase 1 (TBK1), which phosphorylates the key transcription factor interferon regulatory factor 3 (IRF3). While IRF3 activation is commonly used as the main indicator for IFN-β transcription triggered by viral infection, IFN-β transcription also requires additional transcription factor complexes, which together with IRF3 make up the IFN-β enhanceosome: the nuclear factor kappa-light-chain-enhancer of activated B-cells (NF-κB) and the activator protein 1 (AP-1) complexes (23). Previous studies addressing IFN induction heterogeneity have proposed different explanations on how this pathway may result in heterogeneity. Some

studies have suggested that promoter firing is inherently stochastic, so that all the components including the transcription factors are active, but promoter firing only happens in some cells (19, 24). One study suggested this was due to differences in the 3D structure of the genome (24), while another was unable to pinpoint the source of the noise and concluded it may have to do with enhanceosome assembly (19). In contrast, Zhao et al. proposed that every step leading to IFN induction is subject to heterogeneous noise, from viral replication to signaling protein activation to abundance of transcription factors (21). However, Zhao et al. did not control for the fact that many genes encoding proteins in the IFN induction pathways are themselves ISGs, and this study also used murine cells which do not require NF-κB for IFN induction (21). Overall, the cellular source of the IFN induction heterogeneity remains poorly defined.

In this study, we used the KSHV lytic infection and caspase inhibition system to further probe the source of heterogeneous IFN-β induction, as it is a robust and sustained system for inducing IFN in the context of a viral infection. We developed a reporter that allows us to separate cells expressing high vs. low levels of IFN-β and found that surprisingly, the canonical IFN induction pathway culminating in IRF3 activation was equally activated in both populations. However, activation or levels of other components of the IFN-β enhanceosome better correlated with IFN-β induction. Thus, in our system, activation of the NF-κB component RelA and baseline levels of the AP-1 component ATF2 may be the limiting factors for IFN-β transcription at the single cell level. Moreover, these findings suggest that that IRF3 serves as the infection signal, while AP-1 and NF-κB provide the barrier to excessive IFN-β, at least in reactivating KSHV-infected BC-3 cells. This study highlights the nuanced mechanics behind the

induction of a key component of our body's antiviral response and identifies specific cellular factors that may contribute to limiting IFN-β induction to a small subpopulation of cells during KSHV infection.

Results

A fluorescent tdTomato reporter driven by a minimal human IFN-β promoter distinguishes cells that express high vs. low levels of IFN-β

Using scRNA-seq, we previously found that a very small fraction of KSHV-infected cells produce IFN-β when the virus is reactivated and caspases are inhibited (6). In the scRNA-seq dataset, we calculated this fraction to be 3.8% of the total population and 6% of the infected cells in the early stage of the lytic cycle. Nonetheless, the rare IFN-β producing cells clustered together in our scRNA-seq data (6), suggesting that they have different characteristics from other cell populations. To identify factors involved in IFN-β regulation, we sought to separate and compare IFN-β producing and non-producing cells. We previously engineered a tdTomato reporter driven by two copies of the 303 bp minimal promoter sequence from the human *IFNB1* gene (Fig. 1A) and created stable BC-3 cell lines with this reporter (BC3-IFN-βp-tdTomato cells) (6). BC-3 cells are latently KSHV-infected B cells isolated from a patient with primary effusion lymphoma (25). The IFN-β promoter sequence was taken from previous luciferase or chloramphenicol acetyltransferase reporters (26-28). tdTomato was selected because it is the brightest fluorescent protein whose signal is well separated from autofluorescence, which appears in the green channel and is high in BC-3 cells (29-32). While our original scRNA-seq study was performed in KSHV-infected epithelial cells, the iSLK.219 system (6), we chose BC-3s for subsequent experiments because

they are more biologically relevant, as B cells, but not epithelial cells, are the target of long-term KSHV infection in patients. Moreover, the virus in iSLK.219 cells expresses GFP and RFP fluorescent reporters (33), which restricts our options for fluorescent markers. In BC-3 cells, the KSHV lytic cycle can be reactivated using the protein kinase C activator TPA. Treating BC3-IFN-βp-tdTomato reporter cells with TPA and the pan-caspase inhibitor IDN-6556 induced tdTomato expression compared to TPA treatment alone, with this expression limited to 2% of the cells when measured by flow cytometry (6). Also, treating BC3-IFN-βp-tdTomato reporter cells with TPA and the pan-caspase inhibitor IDN-6556 induced IFN-β mRNA expression compared to no treatment, TPA alone, or the caspase inhibitor alone (Fig. 1C).

To isolate cells expressing high and low IFN-β levels, we subjected the lytically reactivated BC3-IFN-βp-tdTomato reporter cells treated with caspase inhibitors to fluorescence-activated cell sorting (FACS) and collected tdTomato-positive and negative cells (Fig. 1A, B). To confirm that tdTomato-based FACS results in the separation of cells based on IFN-β expression status, we measured tdTomato and IFN-β RNA levels in the sorted samples. Importantly, we found that the endogenous IFN-β transcript was enriched in the tdTomato+ cells and depleted in the tdTomato- cells, as was tdTomato mRNA (Fig. 1D, E). Because KSHV reactivation rates can be variable, we confirmed that all our experiments showed robust activation of the lytic cycle by ensuring that a high percentage of cells produced the KSHV lytic protein ORF45 (Fig. 1F) and that there was clear induction of early KSHV lytic gene ORF50 in cells treated with TPA or TPA and caspase inhibitors (Fig. 1G). Sorting for IFN-β high and low cells indicated no correlation between ORF50 and IFN-β expression (Fig. 1H) indicating that

lytic cells were found in both populations, as we expected based on the scRNA-seq. While TPA-mediated reactivation is the most commonly used method of reliably reactivating KSHV in primary effusion lymphoma cell lines such as BC-3 cells (34, 35), TPA has other pleiotropic effects such as driving activation of multiple signaling pathways involved in growth, apoptosis, and differentiation in different cell types through activation of protein kinase C (36, 37). Therefore, to ensure that the use of TPA did not confound our studies, we measured IFN induction in an uninfected EBV and KSHV-negative B cell lymphoma line, BJAB cells (38). BJAB cells are commonly used as an uninfected control for experiments with BC3 cells and other primary effusion lymphoma cell lines (39, 40). We found that neither IFN-β nor the type III IFN IFN-λ1 were induced after TPA or TPA and caspase inhibitor (IDN-6556) treatment in uninfected BJAB cells (Fig. 1I, J). Therefore, we concluded that the IFN induction in BC-3 cells was indeed due to KSHV lytic reactivation and virus sensing, not TPA addition, and that this system could be used for further experiments.

IFN-β signaling also potentiates its own transcription through upregulation of IFN-induction pathway components (41). Indeed, in the scRNA-seq experiment, blocking IFN responses with an anti-IFN antibody cocktail reduced the number of IFN-β-positive cells (6). Therefore, to specifically analyze the “first responder” cells in which IFN-β was only induced by pathogen sensing, without any feed-forward response, we treated the cells with the anti-IFN antibody cocktail. Consistent with the scRNA-seq results in iSLK.219 cells, we still observed IFN-β induction in the lytic BC-3 cells treated with caspase inhibitors after antibody treatment, although it was decreased (Fig. 2A). FACS based on the tdTomato reporter also successfully enriched the rare IFN-β producing

cells under these conditions (Fig. 2B, C). We also still detected reactivation, measured by ORF45 staining or induction of the lytic gene ORF50, in the presence of the antibody cocktail (Fig. 2D, E). Again, sorting for IFN-β high and low cells indicated no correlation between ORF50 and IFN-β expression (Fig. 2F).

The enrichment of IFN-β mRNA in cells selected for tdTomato expression (with and without blocking IFN paracrine signaling) demonstrates that our IFN-βp-tdTomato reporter recapitulates heterogeneous expression of the native IFN-β transcript. High levels of reporter expression corresponded to high levels of IFN-β mRNA. Moreover, these results demonstrate that FACS of the BC3-IFN-βp-tdTomato reporter line allows us to separate cells producing high and low levels of IFN-β within a population and to analyze differences between them.

IFN-β is not stochastically induced

Some groups have proposed that heterogeneous expression of IFN-β may be generated by stochasticity of IFN-β promoter firing (19, 24). This model posits that the signals and activated proteins needed for IFN-β induction are present in all infected cells, but transcription of IFN-β only occurs stochastically in some cells. To test this hypothesis, we took advantage of the fact that pathogen sensing often induces type III IFNs like IFN-λ1 in addition to type I interferons. The signaling cascade and transcription factors that regulate IFN-β and IFN-λ1 are largely the same (42), so any heterogeneity in upstream signaling should affect their induction in a coordinated way (Fig. 3A). The IFN-β promoter is bound by AP-1, IRF3, and NF-κB, and the IFN-λ1 promoter by IRF3 and NF-κB (43). However, since IFN-β and IFN-λ1 have separate promoters and are located on different chromosomes, stochastic noise in assembly of

the transcription factors or other aspects of promoter firing (19) would differentially affect them. Contrary to the stochasticity model, our results suggested that IFN-β and IFN-λ1 were induced in the same cells. In the previously published scRNA-seq results, IFN-λ1 was also induced in iSLK.219 cells upon lytic reactivation and caspase inhibitor treatment, and in the same rare cell populations that expressed IFN-β, indicating a shared regulation mechanism (6). We have since performed further analysis of the scRNA-seq data and found that indeed expression of IFN-λ1 and IFN-β was highly correlated at the single cell level. In fact, no other transcript showed closer correlation using Seurat function for gene enrichment, FindAllMarkers, on single cells separated by IFN-β expression. We also analyzed IFN-λ1 expression after sorting BC3-IFN-βp-tdTomato cells, using the same samples in which we analyzed IFN-β expression in Fig. 1. Like IFN-β, IFN-λ1 was induced in BC-3 lytic cells treated with the caspase inhibitor IDN-6556 (Fig. 3B). Moreover, IFN-λ1 was enriched and depleted in concert with IFN-β in the tdTomato positive and negative cells, respectively (Fig. 3C. compared to IFN-β in the same samples, Fig. 1D). This result indicates that IFN-β and IFN-λ1 were expressed in the same subset of cells. Similarly to IFN-β, IFN-λ1 induction can also be potentiated in response to IFN signaling by a feed-forward loop (Fig. 3A), so we repeated the experiments in the presence of anti-IFN antibodies to block paracrine signaling and checked that the correlation was not a response to IFN. While this treatment did reduce IFN-λ1 induction dramatically, the pattern of IFN-λ1 and IFN-β co-expression was also observed in the absence of IFN responses, as the IFN-λ1 transcript was enriched in the tdTomato+ cells (Fig. 3E), where IFN-β was also enriched (Fig. 2B, same samples). These results stand in contrast to MxA, a classical ISG. MxA is induced in the lytically

reactivated and caspase inhibitor-treated cells (Fig. 3F), i.e. under conditions where IFNs are secreted, as expected for an ISG. Moreover, also as expected, anti-IFN antibodies block MxA induction (Fig. 3H; anti-IFN antibodies were only added to the lytic + caspase inhibitor condition, as this is the condition in which we see high IFN production). This result also confirms that the antibody treatment blocks IFN responses. However, unlike IFN-λ1, MxA is not enriched in sorted cells in the presence or absence of paracrine signaling, demonstrating that the coordinate expression of IFN-λ1 and IFN-β was not related to IFN responses and IFN signaling potentiation of IFN-λ1 induction (Fig. 3G, I). These results are consistent with the scRNA-seq data in iSLK.219 cells, where we detected IFN-induced ISG expression in all cell clusters, not just the ones producing IFN-β, whereas IFN-λ1 was mostly detected in IFN-β-producing clusters (6). Therefore, we conclude that IFN-β and IFN-λ1 are not stochastically transcribed but coordinately regulated. Moreover, the fact that they are expressed in the same rare subset of KSHV-infected cells suggests that heterogeneity in the same upstream determinants leads to cell-to-cell differences in type I and III IFN induction.

TBK1 and IRF3 activity does not explain IFN-β heterogeneity

The results above suggested that activation of the IFN-β induction pathway, rather than IFN-β transcription, was heterogeneous. However, there are several signaling steps in the IFN-β induction pathway that could be the bottleneck determining whether cells transcribe IFN-β. Therefore, we monitored activation of the IFN-β induction pathway, particularly the later steps of kinase and transcription factor activation. Using inhibitors for cGAS and TBK1, we confirmed IFN-β and IFN-λ1

induction is driven by the cGAS-STING pathway through the TBK1 kinase in KSHV-reactivating BC-3 cells (Fig. 4A, B), similarly to what we had previously found in the epithelial iSLK.219 cells (6, 20). We thus tested whether TBK1 was activated only in the cells that induced IFN-β by comparing levels of TBK1 phosphorylation in lytically reactivated, caspase inhibitor-treated cells sorted based on tdTomato status. To ensure the antibodies detected the correct epitopes, we used poly(I:C)-treated A549 cells as positive controls for TBK1 phosphorylation. In every experiment, tdTomato-based sorting resulted in the expected enrichment and depletion of IFN-β mRNA in tdTomato+ and tdTomato- cells, respectively (RNA measurements are shown in Fig. 1D). However, surprisingly, we observed no difference in activated (phosphorylated) TBK1 between IFN-β high and low cells (Fig. 4C, D). Since TBK1 phosphorylates and activates the well-characterized IFN-β transcription factor IRF3, we also tested whether IRF3 was differentially activated in the IFN-β high vs. low cells (i.e. tdTomato+ and -), again using poly(I:C)-treated A549 cells as a positive staining control. Like TBK1, we observed no difference in IRF3 phosphorylation between the two populations (Fig. 4C, E). We also observed no difference in TBK1 and IRF3 phosphorylation between IFN-β high and low cells when we blocked autocrine and paracrine IFN-β signaling with anti-IFN antibodies (Fig. 4F-H). All these experiments were conducted on samples in which we had verified IFN-β mRNA enrichment in the tdTomato+ sorted cells (Fig. 2B). Therefore, while both TBK1 and IRF3 were active in lytic cells treated with caspase inhibitors, their activation alone was not predictive of IFN-β induction. To ensure that the lytic cycle-inducing TPA treatment was not a confound for these experiments, we treated uninfected BJAB cells with the same drugs (TPA and the caspase inhibitor IDN-6556). We confirmed that

these treatments did not activate TBK1 and IRF3 in the absence of KSHV infection (Fig. 4I). These results indicate that the canonical IFN induction pathway is activated in many, likely most, lytically reactivated KSHV-infected BC-3 cells when caspases are inhibited. However, an additional factor besides IRF3 activation keeps IFN-β induction limited to a small fraction of the population.

AP-1 expression and NF-κB activation correlate with IFN-β induction and may drive heterogeneity

IRF3 activation is assumed to lead to IFN-β transcription, and phosphorylation of IRF3 is commonly used as a proxy for IFN induction. However, the IFN-β enhanceosome contains two additional transcription factor complexes: AP-1 and NF-κB (Fig. 5A) (44-46). While the AP-1 and NF-κB complexes can be composed of many different members depending on the context, AP-1 complexes formed by c-Jun and ATF2 and NF-κB complexes formed by the RelA/p65 and NFKB1/p50 subunits have been specifically linked to IFN-β transcription during viral infections (46). NF-κB and IRF3 are also verified transcription factors for IFN-λ1 (47). How AP-1 and NF-κB are activated during IFN-β induction and their relation to activation of cGAS and other PRRs is not well understood. Given that IRF3 activation did not explain IFN-β heterogeneity, we considered the possibility that AP-1 and/or NF-κB might be determinants of heterogeneous IFN-β induction in our system. We previously reported that expression of NF-κB family members were enriched in IFN-β-expressing cells based on single cell RNA-seq analysis of KSHV-infected epithelial cells treated with caspase inhibitors (6). We reanalyzed the scRNA-seq dataset to test whether this was also the case for the

AP-1 components. To further explore the relationship between IFN-β and these transcription factors, we separated the cells from the two IFN-β expressing clusters by IFN-β status. The AP-1 component ATF2 was enriched in both IFN-β-positive and negative cells within the IFN-β expressing clusters, while the AP-1 component c-Jun and the NF-κB components RelA and NFKB1 were specifically enriched in the IFN-β-positive cells (Fig. 5B). These enrichments were particularly evident when anti-IFN antibodies were added to block paracrine and autocrine signaling, because most of these genes were also induced by IFN-β signaling (Fig. 5C). To note, there was an enrichment of IRF3 mRNA in the IFN-β-producing cells in the scRNA-seq data (Fig. 5B-C), even though we did not detect enrichment at the protein level in BC-3 cells (Fig. 4C, F). We also observed that after blocking paracrine signaling, IFN-β expression was reduced in one of the IFN-β expressing clusters (Fig. 5B-C). This cluster may represent "secondary responder" cells in which IFN-β is induced mainly after the initial IFN signaling potentiates the sensitivity of the cells, while the other cluster may comprise "first responder" IFN-β-producing cells (Fig. 3A). These results are consistent with the overall reduction in IFN-β induction that we saw upon addition of the anti-IFN antibodies (Fig. 2A).

We then tested whether NF-κB and AP-1 were similarly enriched at the protein level in BC-3 cells expressing high levels of IFN-β. To reduce confounds from paracrine signaling observed in the scRNA-seq results, we performed the FACS experiments with anti-IFN blocking antibodies. Interestingly, we observed an enrichment in the AP-1 component ATF2 in tdTomato+ cells, indicating that ATF2 levels are higher in cells that express high levels of IFN-β (Fig. 5D, E). Total ATF2 levels did not change between

conditions in bulk samples, indicating that ATF2 expression was not induced at the bulk level during infection and/or by caspase inhibitor treatment. Instead, these results suggest that basal expression of ATF2 may be variable and that IFN-producing cells had higher ATF2 levels prior to lytic reactivation (Fig. 5D). It is also possible that ATF2 levels are induced only in the rare cells that express IFN. ATF2 levels were not changed by TPA and/or caspase inhibitor treatment in uninfected BJAB cells (Fig. 5G). Levels of the other AP-1 component, c-Jun, were variable across replicates, but in two out of three replicates a unique shorter isoform was detected in the sorted IFN-β high cells (Fig. 5D). However, this shorter c-Jun isoform was also induced by treatment of uninfected BJAB cells treated with TPA and caspase inhibitors, suggesting that its appearance may be unrelated to viral replication and IFN induction (Fig. 5H), as IFN-β is not induced in uninfected cells (Fig. 1K). In addition, we also found that IFN-β high cells are enriched in phosphorylated RelA, one of the NF-κB components, whereas there was little to no phosphorylated RelA in the IFN-β low cells (Fig. 5I-J). This result points to RelA activation only in IFN-β high cells. RelA phosphorylation was not induced by TPA and/or caspase inhibitor treatment in uninfected BJAB cells at the same timepoint (two days after TPA addition), indicating this was specific to infected cells (Fig. 5K). Overall, these results indicate that ATF2 and p-RelA likely have important roles in cell-specific IFN-β induction. Particularly elevated ATF2 levels may be needed for IFN-β induction, while RelA is likely activated in response to a stimulus to potentiate IFN transcription in the small subset of IFN producing cells (Fig. 6).

Discussion

In this study, we investigated underlying differences between cells that induce high vs. low levels of IFN-β in the context of KSHV infection and caspase inhibition. We reveal that the IFN-β enhanceosome components AP-1 and NF-κB, but not IRF3, are likely to determine whether individual cells induce IFN-β during KSHV and caspase inhibition. Protein levels of the AP-1 factor ATF2 and phosphorylation of the NF-κB factor RelA were higher in cells that express higher levels of IFN-β compared to cells that express low IFN-β. ATF2 levels were not upregulated under IFN-inducing conditions in bulk samples, suggesting that sorting for cells with high IFN-β enriched for cells with high ATF2. Therefore, this result points to a model whereby ATF2 heterogeneity precedes viral reactivation, and only cells with higher ATF2 respond to pathogen cues by turning on IFN-β. In contrast, RelA was only activated under IFN-inducing conditions, which suggests a possible bottleneck to its activation in most cells. Our findings thus support a model in which IFN-β inducibility during KSHV lytic replication is limited to a rare fraction of cells with elevated baseline ATF2 levels and activated NF-κB. While IRF3, AP-1, and NF-κB have long been known to regulate IFN transcription, the cell-to-cell heterogeneity in their levels and activation has not previously been reported. Moreover, this is the first description of a possible role for AP-1 and NF-κB in controlling which individual cells make IFN, despite cGAS-to-IRF3 signaling being on in almost all infected cells in the population.

Host regulation of IFN-β is important given its potent effects on both the host and pathogen through autocrine and paracrine induction of hundreds of ISGs. Insufficient induction of ISGs can lead to susceptibility to infection, while excessive IFN-related inflammation can lead to autoimmune disorders and excessive tissue damage. A

system in which the barrier for IFN-β induction is very high may provide an appropriate level of innate immune alarm by limiting IFN-β expression to a small fraction of infected cells. The fact that many viral infections display heterogeneous IFN induction in a way that is not fully explained by viral factors (11, 19, 21, 22), in combination with our results, suggests that an important part of the mechanism of IFN regulation is rooted in cellular heterogeneity. Furthermore, heterogeneous expression of other cytokines such as IL-2 (48), IL-4 (49, 50), IL-5 (51), and IL-10 (52) has been reported, suggesting this is an important mode of immune regulation.

Interestingly, while IRF3 and TBK1 are required for IFN induction following PAMP/DAMP signaling, here we found they are not sufficient for IFN-β induction. Although IRF3 activation is often used as a proxy for IFN-β induction, especially in studies of viral infections, our results indicate that this one-to-one relationship is not true at the level of individual cells. Indeed, both TBK1 and IRF3 appear to be activated regardless of the IFN-expressing status of the cells. Most likely, the upstream components of the IFN induction pathway, including the PRR (cGAS in this case), are also activated regardless of the IFN status of the cells. Instead, our results point to the other IFN-β enhanceosome factors, AP-1 and NF-κB, as the potential limiting factors that determine IFN-β induction in individual cells. We propose a model where activation of IRF3 is the main signal that reports on the presence of an infection, while the main function AP-1 and NF-κB is to provide an additional barrier to limit IFN-β induction to a small subset of cells among an infected population.

The regulation of AP-1 and NF-κB during IFN responses is not as well characterized as the activation of IRF3. For AP-1, our results suggest that differences

may precede infection, because at the bulk level there is no clear change in ATF2 levels. Therefore, the simplest interpretation for our results (Fig. 5D) is that some cells have higher ATF2, and these cells are more abundant in the IFN-producing pool. We were unable to detect changes in phosphorylation of ATF2 and c-Jun under IFN-inducing conditions, suggesting this activation step may be dispensable in our system (data not shown). In contrast, NF-κB is likely activated in a subset of cells under IFN-inducing conditions. While IRF3 and NF-κB may both be activated downstream of STING based on previous studies (53, 54), the fact that NF-κB is only phosphorylated in IFN-β high cells while IRF3 is also phosphorylated in IFN-β low cells indicates that there must be a heterogenous bottleneck specifically for NF-κB activation. We attempted to use inhibitors of the IκB kinases α and β (IKKα/β), which activate RelA under other conditions (55-57), to test whether they are required for RelA phosphorylation and IFN-β induction in KSHV infection. However, IKKα/β inhibitors strongly inhibited KSHV reactivation (data not shown), which precluded testing of effects on IFN-β induction. We also tested inhibitors of the transforming growth factor-β-activated kinase 1 (TAK1), which, in many signaling pathways, is upstream of IKKα/β (58), but this inhibitor had no effect on IFN-β levels or phosphorylation of RelA in our system (data not shown). Therefore, we still do not know whether IKKα/β or other kinases phosphorylate NF-κB during IFN-β induction in our system.

While this study has shed light on the expression mechanics of IFN-β during KSHV infection, it is possible that the mechanism of IFN heterogeneity is different for other viral infections and cell types. Although IFN heterogeneity is a widespread feature of viral infection, reported by every study we have encountered, the PRRs and signaling

pathways that lead to IFN induction vary (6-18, 59). Moreover, IFN-β expression patterns appear to differ between cell types. For example, a larger proportion of dendritic cells express IFN-β upon infection (19, 60, 61) compared to other cell types such as fibroblasts and epithelial cells (6-16). Flexibility in tailoring the IFN response to factors such as cell type, viral load, and PAMP type is likely evolutionarily beneficial in mounting an appropriate immune response. More studies identifying the determinants of IFN expression are needed to parse out the ubiquity vs. uniqueness of our findings.

Although our findings suggest there is a high barrier to IFN-β induction, results from studies using Sendai virus suggest that heterogeneity of IFN-β induction is not due to a complete inability of some cells to induce IFN-β. Infection with a highly inflammatory strain of Sendai virus (Cantell) induced IFN-β expression in 99% of infected A549 cells at high multiplicity of infection (11, 61). In comparison, only 0.48% of A549 cells expressed IFN-β during infection with influenza A virus (11). This indicates that IFN-β regulation can be overridden given excessive stimuli such as the defective-interfering viral genomes that characterize the Sendai virus strain Cantell (62). These observations also suggest that the strength or abundance of the stimulus may matter. Indeed, strong IFN inducers like Newcastle Disease Virus, Sendai virus strain Cantell, or the potent PAMP mimetic poly(I:C) induce IFN-β in a larger proportion of cells (10-99%) (21, 22, 59, 60, 63-66) compared to other viral infections and treatments (1-10%) (6-17). Unfortunately, we have been unable to test whether the relationship between stimulus strength and percentage of IFN-expressing cells is also true in KSHV-reactivating BC-3 cells, as we have not identified a stronger stimulus for these cells. To isolate the cells that express IFN-β, the cells need to be active and viable for long enough for the

tdTomato fluorescent protein to express and accumulate to detectable levels. Commonly used IFN-inducing stimuli (poly(I:C), 2’3’-cGAMP, STING agonist diABZI, TLR7 agonist imiquimod, and plasmid DNA) either did not induce IFN-β expression in BC-3 cells or induced cell death before we could measure tdTomato production (data not shown). IFN-β induction through KSHV reactivation and caspase inhibition allows for sustained IFN-β induction without inducing cell death, which gives us a unique tool to study the elusive phenomena of cellular heterogeneity during IFN-β induction.

While our scRNA-seq data did not reveal any correlations between viral genes and IFN-β expression (6), technical limitations of short read sequencing may have missed some important components. For example, the scRNA-seq would not have captured mutations in KSHV that may have risen in individual cells. Moreover, the sequencing method was 3’ end directed, and many mRNAs in KSHV share 3’ end sequences, preventing accurate measurement of some viral genes. KSHV has evolved a large arsenal of proteins that antagonize IFN signaling. KSHV ORF52 can prevent cGAS activation by sequestering DNA substrates by phase separation mechanism (67), and a truncated and therefore cytoplasmic form of KSHV LANA also inhibits cGAS (68). KSHV ORF33 aids in inactivating the cGAS-adaptor STING (69). One study found that the KSHV homolog of human IRFs vIRF1 inhibits IFN-β by preventing STING and TBK1 activation during KSHV reactivation in iSLK.219 cells (70). However, these viral factors all act upstream of IRF3 activation, which is still active even in IFN-β-low cells in our system, and are therefore unlikely to explain IFN induction heterogeneity. KSHV vIRFs have also been implicated in regulating IFNs at the transcriptional level. Studies on KSHV vIRF3 and vIRF4 have found that these inhibit IRF7, which is important for

484 inducing secondary responder cells (71, 72). A study on KSHV vIRF2 found that it
485 induces IRF3 degradation via caspase-3 (73). Another study found KSHV vIRF1 inhibits
486 IFNA4 induced by Newcastle Disease Virus in murine cells by preventing p300 from
487 binding to IRF1 and IRF3 (74). KSHV vIRF1 also binds CBP/p300 to prevent IRF3
488 complex formation on the IFN-β promoter during Sendai Virus infection in 293T cells
489 (75). Potentially, these events could create a barrier downstream of IRF3
490 phosphorylation, but this remains to be tested. Also, there has been no reports of any
491 KSHV factor that regulates AP-1 levels or blocks NF-κB activation, so there is no
492 obvious viral explanation for the heterogeneity we observe for these factors.

493 There are some limitations to our study. First, our reporter system likely does not
494 fully recapitulate native IFN-β mRNA expression and kinetics. The minimal IFN-β
495 promoter lacks the native chromatin environment and potential long range promoter
496 elements. The reporter also lacks the native 3' untranslated region of the IFN-β mRNA,
497 which makes this mRNA unstable. Also, it is likely that only cells with sustained IFN-β
498 promoter activity were detected and sorted, as sufficient accumulation of the tdTomato
499 protein is needed for FACS. However, despite these imperfections, we were able to
500 successfully separate the cells that expressed high and low levels of IFN-β at the time
501 of sorting (Fig. 1D). Also, while our results point to cellular heterogeneity as a major
502 determinant of IFN-β regulation, we cannot completely rule out the possibility that the
503 heterogeneity of AP-1 and NF-κB is regulated by the virus, as described above. Lastly,
504 while TPA is a very effective inducer of lytic KSHV reactivation and is commonly used in
505 KSHV research (34), it is also a known inducer of NF-κB. This is a potentially
506 confounding variable. Our concerns are reduced by the fact that treatments that induce

IFN-β in infected BC-3 cells do not induce IFN-β or phosphorylation of TBK1, IRF3, or RelA in the uninfected BJAB cells at comparable time points, indicating viral reactivation rather than TPA treatment drives signaling changes in our system (Figs. 1I, 4I, 5K). Moreover, to date, all our results are consistent between the BC-3 and iSLK.219 KSHV-infected cell lines, even though iSLK.219 cells are not treated with TPA to induce the lytic cycle. This also suggests that our results are not simply due to TPA effects.

Despite the described limitations, this study points to a new model of heterogeneous type I interferon transcription during viral infection as the result of inherent cellular heterogeneity in protein levels and protein activation. More studies are needed to pinpoint the earliest source of the heterogeneity and to examine the mechanism of enrichment and activation of AP-1 and NF-κB in the context of antiviral responses.

Materials and Methods

Cell lines, reagents, and treatments

All cells were cultured at 37°C and 5% CO_2. HEK293T cells were grown in Dulbecco's modified Eagle's medium (DMEM; Life Technologies) supplemented with 10% fetal bovine serum (FBS; Hyclone). BC-3 cells and derivatives were maintained at a density of $5x10^5$ cells/mL in Roswell Park Memorial Institute medium (RPMI; Life Technologies) supplemented with 20% FBS, 2 mM GlutaMAX (Gibco), and 55 µM β-mercaptoethanol (BME; Gibco). BC-3-IFN-βp-tdTomato cells were generated as described in Lent, Tabtieng, et al., 2022 (6). The transduced cells were purposefully not clonally selected, because KSHV reactivation can be variable among KSHV-infected cells in a population and clonal selection can result in artifacts. For reactivation, BC-3 and BC-3-IFN-βp-tdTomato cells were seeded at a density of $5x10^5$ cells/mL and treated with 20 ng/mL TPA (12-O-tetradecanoylphorbol-13-acetate; MilliporeSigma 5244001MG) in dimethylsulfoxide (DMSO; Sigma Aldrich Fine Chemicals Biosciences). Where indicated, cells were treated with vehicle (DMSO), 10 µM IDN-6556 (Emricasan; Selleck Chemical LLC S777525MG), a mixture of neutralizing antibodies against type I IFNs at 1:2000 dilution (PBL Assay Science 39000-1), 10 µM TBK1 inhibitor (MRT67307; Medchemexpress LLC HY130185MG), and/or 10 µM cGAS inhibitor (G140; Invivogen inh-g140).

Fluorescence-activated cell sorting

100 mL of BC-3-IFN-βp-tdTomato cells were seeded at a density of $5x10^5$ cells/mL and treated with TPA, IDN-1665, and, where indicated, an anti-IFN antibody mixture as described above. After two days, they were collected and stained with 1 µg/mL DAPI (4',6-Diamidino-2-Phenylindole, Dihydrochloride) stain (Invitrogen, D1306) for 5 minutes at room temperature. They were then washed in phosphate buffer saline (PBS; Life Technologies) and filtered through a 35 µm strainer (Chemglass Life Sciences CLS4380009) and sorted based on tdTomato fluorescence on a BD FACSAria III at the University of Wisconsin Carbone Cancer Center Flow Cytometry Laboratory core facility. The DAPI stain was used to remove dead cells from the analysis, as in the absence of permeabilization it only stains dead cells. Gates for tdTomato fluorescence were drawn based on a negative control consisting of BC-3 cells that lack the reporter. BC-3 cells lacking the reporter were treated in the same way as the sorted reporter cells. In each experiment, about $80x10^6$ cells were sorted. $3x10^6$ tdTomato+ and $12x10^6$ tdTomato- cells were collected in each experiment. Sorted cells were pelleted and resuspended in 1 mL of PBS. 100 µL of cell suspension were used for RNA extraction and 900 µL for protein extraction. Bulk controls were prepared in parallel using 4 mL of BC-3-IFN-βp-tdTomato cells seeded at a density of $5x10^5$ cells/mL and treated with TPA, IDN-6556, anti-IFN antibodies, TBK1, or cGAS inhibitors (or corresponding vehicle) as indicated for 2 days. The bulk control cells were pelleted and resuspended in 1 mL of PBS. 50 µL of cell suspension were used for RNA extraction, 450 µL for protein extraction, and 500 µL for flow cytometry to determine KSHV reactivation efficiency.

RT-qPCR

RNA samples were collected from BC-3 or BC-3-IFN-βp-tdTomato cells reactivated for 2 days as described above or treated with vehicle. For experiments involving sorting, a fraction of the sorted cells was used as described in the Fluorescence-activated cell sorting section. For experiments not involving sorting, 4 mL of BC-3/ BC-3-IFN-βp-tdTomato cells were collected as described in the same section for bulk control samples. In both cases, cells to be lysed were pelleted by centrifugation and resuspended in RNA lysis buffer (Zymo research). Total RNA was extracted using the Quick-RNA MiniPrep kit (Zymo research) following the manufacturer's protocol. cDNA was prepared using an iScript cDNA synthesis kit (Bio-Rad) following the manufacturer's protocol. Real-time quantitative PCR (RT-qPCR) was performed using iTaq Universal SYBR green Supermix (Bio-Rad) following the manufacturer's protocol in CFX Duet Real-Time PCR System (Bio-Rad). For KSHV gene ORF50, cDNA was prepared using AMV RT (Promega) following the manufacturer's protocol using 1 pmol reverse primer for ORF50 to select for transcripts from the correct strand of the genome. No-template and no-RT controls were included in each replicate experiment, and experiments were only included if these controls showed negligible amplification rates. In all cases, target mRNA levels were normalized to levels of 18S rRNA as an internal standard. CFX Maestro software was used to analyze the data. Primers specific for each gene:

Target	Forward 5' → 3'	Reverse 5' → 3'	ref
Human IFN-β	GTCAGAGTGGAAATCCTAAG	ACAGCATCTGCTGGTTGAAG	(76)
Human 18S rRNA	GTAACCCGTTGAACCCCATT	CCATCCAATCGGTAGTAGCG	(77)
Human MxA	ATCCTGGGATTTTGGGGCTT	CCGCTTGTCGCTGGTGTCG	(78)
tdTomato	ACATCCCCGATTACAAGAAGC	TTGTAGATCAGCGTGCCGTC	(79)
Human IFN-λ1	CGCCTTGGAAGAGTCACTCA	GAAGCCTCAGGTCCCAATTC	(80)
KSHV ORF50	ACCAAGGTGTGCCGTGTAGAGATT	AGCCTTACGCTTCTTTGAGCTCCT	(81)

Protein analysis

Protein samples were collected from BC-3/BC-3-IFN-βp-tdTomato cells reactivated for 2 days as described above or treated with vehicle. For experiments involving sorting, a fraction of the sorted cells was used as described in the Fluorescence-activated cell sorting section. For samples not involving in sorting, 4 mL of BC-3/ BC-3-IFN-βp-tdTomato cells were used and collected as described for bulk control samples in that section. In both cases, cells to be lysed were pelleted by centrifugation and resuspended in an NP-40-only buffer (50 mM Tris-HCl pH 7.4, 150 mM NaCl, 1 mM EDTA, 0.5% NP-40) supplemented with a broad-spectrum protease inhibitor mixture (Thermo Scientific A32955) and a broad-spectrum phosphatase inhibitor mixture (Thermo Scientific A32957). Protein concentration was determined by Bradford method (Bio-Rad 5000006). Between 10 and 20 µg of protein were loaded on each gel. Laemmli buffer (Bio-Rad) was added to samples before incubation at 95°C for 5 min. Samples were separated by SDS-PAGE and transferred to polyvinylidene difluoride membranes (PVDF; Fisher Scientific IPFL00010) using the semi-dry Trans-Blot Turbo Transfer System (Bio-Rad). Membranes were blocked in 5% bovine serum albumin (BSA; Fisher BioReagents BP1600-100) in Tris-Buffer Saline with 0.1% Tween (TBST). All antibodies used were diluted 1:1000 in 5% BSA in TBST for staining. The following Cell Signaling Technologies antibodies were used: IRF3 (D6I4C, no.11904), phospho-IRF3 Ser386 (E7J8G, no.37829), TBK1 (D1B4, no.3504), phospho-TBK1 Ser172 (D52C2, no.5483), ATF2 (D4L2X, no.35031), c-Jun (60A8, no.9165), NF-κB p65/RelA (D14E12, no.8242), phospho-NF-κB p65/RelA Ser536 (93H1, no.3303). In addition, antibodies against β-actin (Abcam, ab8229) were used to stain for loading controls. Secondary horseradish

peroxidase (HRP)-conjugated antibodies (goat anti-rabbit and rabbit anti-goat IgG) were purchased from Southern Biotechnology (no.4030-05, no.OB6106-05) and used at 1:5000 in 5% BSA in TBST. All membranes were exposed using SuperSignal West Pico PLUS Chemiluminescent Substrate (Thermo Scientific) and imaged with an iBright FL1000 imaging system (Thermo Scientific). Protein quantification from western images was done using Image J (82).

Flow cytometry analysis

BC-3-IFN-βp-tdTomato cells were fixed with 4% paraformaldehyde (PFA; Electron Microscopy Sciences) in PBS for 15 min at room temperature and washed twice with PBS. Then, the cells were permeabilized by incubating in ice cold 90% methanol diluted in 0.5% BSA in PBS for 5 min on ice and washed twice with 0.5% BSA in PBS. For assessment of reactivation efficiency, cells were stained for a KSHV lytic infection marker, ORF45. They were incubated with antibodies against KSHV ORF45 (Thermo Fisher MA514769) at 1:100 dilution for 1 hr at room temperature, washed twice, and then stained with Alexa Fluor 647 (AF647)-conjugated secondary antibody at 1:500 dilution (Thermo Fisher A21236) for 30 min at room temperature in the dark. 0.5 % BSA in PBS was used for all incubations and washes. Cells were collected by centrifugation at 500 x *g* for 5 min between all washes/incubation. After two washes, cells were resuspended in 0.5% BSA in PBS and filtered through a 35 µm strainer (Chemglass Life Sciences CLS4380009) for analysis. Fluorescence was quantified by flow cytometry on a Thermo Fisher Attune NxT V6 cytometer at the UW-Madison Carbone Cancer Center Flow Cytometry Laboratory. AF647 fluorescence was gated based on the corresponding

latently infected and vehicle (DMSO)-treated cells. $3x10^6$ events were collected per sample. FlowJo 10.8.2 was used for the data analysis.

Single cell RNA sequencing analysis

A dataset obtained from iSLK.219 cell samples previously published in Lent, Tabtieng, et al., 2022 (6) (GSE190558) was re-analyzed in the current study by extracting prepared Seurat matrices and manually selecting genes of interest.

Statistics

All statistical analysis was performed using GraphPad Prism version 10.3.0 or later (GraphPad Software, Boston, MA USA; www.graphpad.com). Statistical significance was determined by One- or Two-way ANOVA followed by a *post hoc* multiple-comparison test (Dunnett or Tukey) when multiple comparisons were required. Statistical analysis of qRT-PCR data was performed on log_2 transformed data to ensure normal distribution (83). Singular outliers were identified using Grubbs' test (alpha = 0.05) for outliers, and removed from Fig. 1I-J, Fig. 2A, and Fig. 3D, F, G. All plots represent mean +/- standard deviation. Figure legends indicate the number of biological replicates used for each experiment. All western blot images are representative of 3 or more independent biological replicates.

Acknowledgements

We thank members of the Gaglia laboratory for suggestions and feedback on the project and the manuscript. We thank the University of Wisconsin Carbone Cancer

Center (UWCCC) Flow Cytometry Laboratory staff for technical and conceptual assistance and services. This work was supported by National Institutes of Health Grant R01 CA268976 to M.M.G. and by the University of Wisconsin-Madison, Office of the Vice Chancellor for Research and Graduate Education with funding from the Wisconsin Alumni Research Foundation. The UWCCC Flow Cytometry Laboratory is supported by the UWCCC Cancer Center Grant P30 CA014520.

References

1. Schoggins JW, Wilson SJ, Panis M, Murphy MY, Jones CT, Bieniasz P, Rice CM. 2011. A diverse array of gene products are effectors of the type I interferon antiviral response. Nature 472.
2. Schoggins JW, Rice CM. 2011. Interferon-stimulated genes and their antiviral effector functions. Curr Opin Virol 1:7.
3. Taft J, Bogunovic D. 2018. The Goldilocks Zone of Type I IFNs: Lessons from Human Genetics. J Immunol 201:7.
4. González-Navajas JM, Lee J, David M, Raz E. 2012. Immunomodulatory functions of type I interferons. Nat Rev Immunol 12:11.
5. Kobayashi KS, Flavell RA. 2004. Shielding the double-edged sword: negative regulation of the innate immune system. J Leukoc Biol 75:6.
6. Tabtieng T, Lent RC, Kaku M, Monago Sanchez A, Gaglia MM. 2022. Caspase-Mediated Regulation and Cellular Heterogeneity of the cGAS/STING Pathway in Kaposi's Sarcoma-Associated Herpesvirus Infection. mBio e0244622.
7. Hamele CE, Russell AB, Heaton NS. 2022. In Vivo Profiling of Individual Multiciliated Cells during Acute Influenza A Virus Infection. J Virol 96.
8. Hein MY, Weissman JS. 2022. Functional single-cell genomics of human cytomegalovirus infection. Nat Biotechnol 40:11.
9. Fiege JK, Thiede JM, Nanda HA, Matchett WE, Moore PJ, Montanari NR, Thielen BK, Daniel J, Stanley E, Hunter RC, Menachery VD, Shen SS, Bold TD, Langlois RA. 2021. Single cell resolution of SARS-CoV-2 tropism, antiviral responses, and susceptibility to therapies in primary human airway epithelium. PLoS Pathog 17.
10. Sun J, Vera JC, Drnevich J, Lin YT, Ke R, Brooke CB. 2020. Single cell heterogeneity in influenza A virus gene expression shapes the innate antiviral response to infection. PLoS Pathog 16.

11. Russell AB, Elshina E, Kowalsky JR, Te Velthius AJW, Bloom JD. 2019. Single-Cell Virus Sequencing of Influenza Infections That Trigger Innate Immunity. J Virol 93.

12. Drayman N, Patel P, Vistain L, Tay S. 2019. HSV-1 single-cell analysis reveals the activation of anti-viral and developmental programs in distinct sub-populations. Elife 8.

13. O'Neal JT, Upadhyay A, Wolabaugh A, Patel NB, Bosinger SE, Suthar MS. 2019. West Nile Virus-Inclusive Single-Cell RNA Sequencing Reveals Heterogeneity in the Type I Interferon Response within Single Cells. J Virol 93.

14. Russell AB, Trapnell C, Bloom JD. 2018. Extreme heterogeneity of influenza virus infection in single cells. Elife 7.

15. Killip MJ, Jackson R, Pérez-Cidoncha M, Fodor E, Randall RE. 2017. Single-cell studies of IFN-β promoter activation by wild-type and NS1-defective influenza A viruses. J Gen Virol 98:7.

16. Pérez-Cidoncha M, Killip MJ, Oliveros JC, Asensio VJ, Fernández Y, Bengoechea JA, Randall RE, Ortín J. 2014. An unbiased genetic screen reveals the polygenic nature of the influenza virus anti-interferon response. J Virol 88:15.

17. Kallfass C, Lienenklaus S, Weiss S, Staeheli P. 2013. Visualizing the beta interferon response in mice during infection with influenza A viruses expressing or lacking nonstructural protein 1. J Virol 87:6.

18. Hu J, Nudelman G, Shimoni Y, Kumar M, Ding Y, López C, Hayot F, Wetmur JG, Sealfon S. 2011. Role of cell-to-cell variability in activating a positive feedback antiviral response in human dendritic cells. PLoS One 6.

19. Hu J, Sealfon S, Hayot F, Jayaprakash C, Kumar M, Pendleton AC, Ganee A, Fernandez-Sesma A, Moran TM, Wetmur JG. 2007. Chromosome-specific and noisy IFNB1 transcription in individual virus-infected human primary dendritic cells. Nucleic Acids Res 35:10.

20. Tabtieng T, Degterev A, Gaglia MM. 2018. Caspase-Dependent Suppression of Type I Interferon Signaling Promotes Kaposi's Sarcoma-Associated Herpesvirus Lytic Replication. J Virol 92.

21. Zhao M, Zhang J, Phatnani H, Scheu S, Maniatis T. 2012. Stochastic expression of the interferon-β gene. PLoS Biol 10.

22. Rand U, Rinas M, Schwerk J, Nöhren G, Linnes M, Kröger A, Flossdorf M, Kály-Kullai K, Hauser H, Höfer T, Köster M. 2012. Multi-layered stochasticity and paracrine signal propagation shape the type-I interferon response. Mol Syst Biol 8.

23. Panne D, Maniatis T, Harrison SC. 2007. An atomic model of the interferon-beta enhanceosome. Cell 129:13.

24. Apostolou E, Thanos D. 2008. Virus Infection Induces NF-kappaB-dependent interchromosomal associations mediating monoallelic IFN-beta gene expression. Cell 134:7.

25. Arvanitakis L, Mesri EA, Nador RG, Said JW, Asch AS, Knowles DM, Cesarman E. 1996. Establishment and characterization of a primary effusion (body cavity-based) lymphoma cell line (BC-3) harboring kaposi's sarcoma-associated herpesvirus (KSHV/HHV-8) in the absence of Epstein-Barr virus. Blood 88.

26. Li K, Chen Z, Kato N, Gale K, Lemon SM. 2005. Distinct poly(I-C) and virus-activated signaling pathways leading to interferon-beta production in hepatocytes. J Biol Chem 280:9.

27. Guo F, Mead J, Aliya N, Wang L, Cuconati A, Wei L, Li K, Block TM, Guo JT, Chang J. 2012. RO 90-7501 enhances TLR3 and RLR agonist induced antiviral response. PLoS One 7.

28. Gentili M, Kowal J, Tkach M, Satoh T, Lahaye X, Conrad C, Boyron M, Lombard B, Durand S, Kroemer G, Loew D, Dalod M, Thery C, Manel N. 2015. Transmission of innate immune signaling by packaging of cGAMP in viral particles. Science 349.

29. Day RN, Davidson MW. 2009. The fluorescent protein palette: tools for cellular imaging. Chem Soc Rev 38:34.

30. Muzumdar MD, Tasic B, Miyamichi K, Li L, Luo L. 2007. A global double-fluorescent Cre reporter mouse. Genesis 45:13.

31. Surre J, Saint-Ruf C, Collin V, Orenga S, Ramjeet M, Matic I. 2018. Strong increase in the autofluorescence of cells signals struggle for survival. Sci Rep 8.

32. Chance B, Schoener B, Oshino R, F. I, Nakase Y. 1979. Oxidation-reduction ratio studies of mitochondria in freeze-trapped samples. NADH and flavoprotein fluorescence signals. J Biol Chem 254:8.

33. Brulois KF, Chang H, Lee ASY, Ensser A, Wong LY, Toth Z, Lee SH, Lee HR, Myoung J, Ganem D, Oh TK, Kim JF, Gao SJ, Jung JU. 2012. Construction and Manipulation of a New Kaposi's Sarcoma-Associated Herpesvirus Bacterial Artificial Chromosome Clone. J Virol 86.

34. Cohen A, Brodie C, Sarid R. 2006. An essential role of ERK signalling in TPA-induced reactivation of Kaposi's sarcoma-associated herpesvirus. J Gen Virol 87:8.

35. Renne R, Zhong W, Herndier B, McGrath M, Abbey N, Kedes D, Ganem D. 1996. Lytic growth of Kaposi's sarcoma-associated herpesvirus (human herpesvirus 8) in culture. Nat Med 2:5.

36. Kikkawa U, Matsuzaki H, Yamamoto T. 2002. Protein kinase C delta (PKC delta): activation mechanisms and functions. J Biochem 132:9.

37. Duquesnes N, Lezoualc’h F, Crozatier B. 2011. PKC-delta and PKC-epsilon: foes of the same family or strangers? J Mol Cell Cardiol 51:9.

38. Menezes J, Leibold W, Klein G, Clemens G. 1975. Establishment and characterization of an Epstein-Barr virus (EBC)-negative lymphoblastoid B cell line (BJA-B) from an exceptional, EBV-genome-negative African Burkitt's lymphoma. Biomedicine 22:9.

39. Sun Z, Xiao B, Jha HC, Lu J, Banerjee S, Robertson ES. 2014. Kaposi's sarcoma-associated herpesvirus-encoded LANA can induce chromosomal instability through targeted degradation of the mitotic checkpoint kinase Bub1. J Virol 88:11.

40. Domsic JF, Chen HS, Lu F, Marmorstein R, Lieberman PM. 2013. Molecular basis for oligomeric-DNA binding and episome maintenance by KSHV LANA. PLoS Pathog 9.

41. Ma F, Li B, Liu S, Iyer SS, Yu Y, Wu A, Cheng G. 2015. Positive feedback regulation of type I IFN production by the IFN-inducible DNA sensor cGAS. 194 4:10.

42. Onoguchi K, Yoneyama M, Takemura A, Akira S, Taniguchi T, Namiki H, Fujita T. 2007. Viral infections activate types I and III interferon genes through a common mechanism. J Biol Chem 282:6.

43. Osterlund PI, Pietilä TE, Veckman V, Kotenko SV, Julkunen I. 2007. IFN regulatory factor family members differentially regulate the expression of type III IFN (IFN-lambda) genes. Immunity 179:9.

44. Lenardo MJ, Fan CM, Maniatis T, Baltimore D. 1989. The involvement of NF-kappa B in beta-interferon gene regulation reveals its role as widely inducible mediator of signal transduction. Cell 57:8.

45. Wathelet MG, Lin CH, Parekh BS, Ronco LV, Howley PM, Maniatis T. 1998. Virus infection induces the assembly of coordinately activated transcription factors on the IFN-beta enhancer in vivo. Mol Cell 1:11.

46. Maniatis T, Falvo JV, Kim TH, Kim TK, Lin CH, Parekh BS, Wathelet MG. 1998. Structure and function of the interferon-beta enhanceosome. Cold Spring Harb Symp Quant Biol 63:12.

47. Iversen MB, Paludan SR. 2010. Mechanisms of type III interferon expression. J Interferon Cytokine Res 30:6.

48. Holländer GA. 1999. On the stochastic regulation of interleukin-2 transcription. Semin Immunol 11:11.

49. Guo L, Hu-Li J, Paul WE. 2004. Probabilistic regulation of IL-4 production in Th2 cells: accessibility at the Il4 locus. Immunity 20:11.

50. Guo L, Hu-Li J, Paul WE. 2005. Probabilistic regulation of IL-4 production. J Clin Immunol 25:9.

51. Kelly BL, Locksley RM. 2000. Coordinate regulation of the IL-4, IL-13, and IL-5 cytokine cluster in Th2 clones revealed by allelic expression patterns. J Immunol 165:5.

52. Calado DP, Paixão T, Holmberg D, Haury M. 2006. Stochastic monoallelic expression of IL-10 in T cells. J Immunol 177:7.

53. Ishikawa H, Barber GN. 2008. STING is an endoplasmic reticulum adaptor that facilitates innate immune signalling. Nature 455:5.

54. Balka KR, Louis C, Saunders TL, Smith AM, Calleja DJ, D'Silva DB, Moghaddas F, Tailler M, Lawlor KE, Zhan Y, Burns CJ, Wicks IP, Miner JJ, Kile BT, Masters SL, De Nardo D. 2020. TBK1 and IKKε Act Redundantly to Mediate STING-Induced NF-κB Responses in Myeloid Cells. Cell Rep 31.

55. Sakurai H, Chiba H, Miyoshi H, Sugita T, Toriumi W. 1999. IkappaB kinases phosphorylate NF-kappaB p65 subunit on serine 536 in the transactivation domain. J Biol Chem 274:4.

56. Mattioli I, Sebald A, Bucher C, Charles RP, Nakano H, Doi T, Kracht M, Schmitz ML. 2004. Transient and selective NF-kappa B p65 serine 536 phosphorylation induced by T cell costimulation is mediated by I kappa B kinase beta and controls the kinetics of p65 nuclear import. J Immunol 172:9.

57. Buss H, Dörrie A, Schmitz ML, Hoffmann E, Resch K, Kracht M. 2004. Constitutive and interleukin-1-inducible phosphorylation of p65 NF-{kappa}B at serine 536 is mediated by multiple protein kinases including I{kappa}B kinase (IKK)-{alpha}, IKK{beta}, IKK{epsilon}, TRAF family member-associated (TANK)-binding kinase 1 (TBK1), and an

unknown kinase and couples p65 to TATA-binding protein-associated factor II31-mediated interleukin-8 transcription. J Biol Chem 279:10.

58. Sakurai H, Miyoshi H, Toriumi W, Sugita T. 1999. Functional interactions of transforming growth factor beta-activated kinase 1 with IkappaB kinases to stimulate NF-kappaB activation. J Biol Chem 274:8.

59. Parekh N, Winship D, Dis EV, Stetson DB. 2024. Regulation and Dynamics of IFN-β Expression Revealed with a Knockin Reporter Mouse. J Immunol 213:11.

60. Shalek AK, Satija R, Shuga J, Trombetta JJ, Gennert D, Lu D, Chen P, Gertner RS, Gaublomme JT, Yosef N, Schwartz S, Fowler B, Weaver S, Wang J, Wang X, Ding R, Raychowdhury R, Friedman N, Hacohen N, Park H, May AP, Regev A. 2014. Single-cell RNA-seq reveals dynamic paracrine control of cellular variation. Nature 510:7.

61. Strahle L, Garcin D, Kolakofsky D. 2006. Sendai virus defective-interfering genomes and the activation of interferon-beta. Virology 351:11.

62. Johnston MD. 1981. The characteristics required for a Sendai virus preparation to induce high levels of interferon in human lymphoblastoid cells. J Gen Virol 56:10.

63. Patil S, Fribourg M, Ge Y, Batish M, Tyagi S, Hayot F, Sealfon S. 2015. Single-cell analysis shows that paracrine signaling by first responder cells shapes the interferon-β response to viral infection. Sci Signal 8.

64. Hwang SY, Hur KY, Kim JR, Cho KH, Kim SH, Yoo JY. 2013. Biphasic RLR-IFN-β response controls the balance between antiviral immunity and cell damage. J Immunol 190:9.

65. Zawatzky R, Maeyer ED, Maeyer-Guignard JD. 1985. Identification of individual interferon-producing cells by in situ hybridization. PNAS 82:5.

66. Enoch T, Zinn K, Maniatis T. 1986. Activation of the human beta-interferon gene requires an interferon-inducible factor. Mol Cell Biol 6:10.

67. Bhowmik D, Tian Y, Wang B, Zhu F, Yin Q. 2022. Structural basis of higher order oligomerization of KSHV inhibitor of cGAS. PNAS 199.

68. Zhang G, Chan B, Samarina N, Abere B, Weidner-Glunde M, Buch A, Pich A, Brinkmann MM, Schulz TF. 2016. Cytoplasmic isoforms of Kaposi sarcoma herpesvirus LANA recruit and antagonize the innate immune DNA sensor cGAS. PNAS 133.

69. Yu K, Tian H, Deng H. 2020. PPM1G restricts innate immune signaling mediated by STING and MAVS and is hijacked by KSHV for immune evasion. Sci Adv 6.

70. Ma Z, Jacobs SR, West JA, Stopford C, Zhang Z, Davis Z, Barber GN, Glausinger BA, Dittmer DP, Damania B. 2015. Modulation of the cGAS-STING DNA sensing pathway by gammaherpesviruses. PNAS 112.

71. Joo CH, Shin YC, Gack M, Wu L, Levy D, Jung JU. 2007. Inhibition of Interferon Regulatory Factor 7 (IRF7)-Mediated Interferon Signal Transduction by the Kaposi's Sarcoma-Associated Herpesvirus Viral IRF Homolog vIRF3. J Virol 81:10.

72. Hwang SW, Kim D, Jung JU, Lee HR. 2017. KSHV-encoded viral interferon regulatory factor 4 (vIRF4) interacts with IRF7 and inhibits interferon alpha production. Biochem Biophys Res Commun 486:6.

73. Aresté C, Mutocheluh M, Blackbourn DJ. 2009. Identification of caspase-mediated decay of interferon regulatory factor-3, exploited by a Kaposi sarcoma-associated herpesvirus immunoregulatory protein. J Biol Chem 284:13.

74. Burysek L, Yeow WS, Lubyova B, Kellum M, Schafer SL, Huang YQ, Pitha PM. 1999. Functional Analysis of Human Herpesvirus 8-Encoded Viral Interferon Regulatory Factor 1 and Its Association with Cellular Interferon Regulatory Factors and p300. J Virol 73.

75. Lin R, Genin P, Mamane Y, Sgarbanti M, Battistini A, Harrington WJ, Barber GN, Hiscott J. 2001. HHV-8 encoded vIRF-1 represses the interferon antiviral response by blocking IRF-3 recruitment of the CBP/p300 coactivators. Oncogene 20:12.

76. Yang Q, Elz AE, Panis M, Liu T, Nilsson-Payant BE, Blanco-Melo D. 2023. Modulation of Influenza A virus NS1 expression reveals prioritization of host response antagonism at single-cell resolution. Front Microbiol 14.

77. Schmittgen TD, Zakrajsek BA. 2000. Effect of experimental treatment on housekeeping gene expression: validation by real-time, quantitative RT-PCR. J Biochem Biophys Methods 46:11.

78. Zhu FX, Sathish N, Yuan Y. 2010. Antagonism of host antiviral responses by Kaposi's sarcoma-associated herpesvirus tegument protein ORF45. PLoS One 5.

79. Valny M, Honsa P, Waloschkova E, Matuskova H, Kriska J, Kirdajova D, Androvic P, Valihrach L, Kubista M, Anderova M. 2018. A single-cell analysis reveals multiple roles of oligodendroglial lineage cells during post-ischemic regeneration. Glia 66:14.

80. Ank N, West H, Bartholdy C, Eriksson K, Thomsen AR, Paludan S. 2006. Lambda interferon (IFN-lambda), a type III IFN, is induced by viruses and IFNs and displays potent antiviral activity against select virus infections in vivo. J Virol 80:9.

81. Rossetto CC, Pari G. 2012. KSHV PAN RNA associates with demethylases UTX and JMJD3 to activate lytic replication through a physical interaction with the virus genome. PLoS Pathog 8.

82. Stael S, Miller LP, Fernández-Fernández ÁD, Van Breusegem F. 2022. Detection of Damage-Activated Metacaspase Activity by Western Blot in Plants. Methods Mol Biol 2447:11.

83. Edmunds RC, McIntyre JK, Luckenbach JA, Baldwin DH, Incardona JP. 2014. Toward Enhanced MIQE Compliance: Reference Residual Normalization of qPCR Gene Expression Data. J Biomol Tech 25:7.

Figure Legends

Figure 1. An IFN-β-promoter driven fluorescent reporter allows isolation of cells expressing high and low levels of IFN-β. A. Diagram of the IFN-βp-tdTomato reporter and sorting strategy. Two copies of the 303 bp minimal promoter sequence for the human IFNB1 gene were cloned in front of the tdTomato fluorophore. This cassette was then introduced in BC-3 cells via lentiviral transduction for stable integration. Cells were sorted based on tdTomato expression and RNA and protein samples were collected from the same experiment. **B-H.** BC3-IFN-βp-tdTomato reporter cells were treated with 20 ng/mL TPA for 48 hours to induce the lytic cycle ("lytic (+TPA)"). Where indicated, the cells were also treated with 10 μM of the pan-caspase inhibitor IDN-6556 ("casp-i"). **B.** Gating strategy for FACS. **C-E, G-H.** IFN-β, tdTomato, and ORF50 mRNA levels were measured by RT-qPCR and normalized to 18S rRNA. For **C-E** and **H**, mRNA levels are plotted relative to the lytic+casp-i sample. For **G,** mRNA levels are plotted relative to the lytic sample. **H.** Cells were stained for KSHV ORF45 and analyzed by flow cytometry. **I-J.** KSHV-negative BJAB cells were treated with 20 ng/mL TPA for 48 hours. Where indicated, the cells were also treated with 10 μM of the pan-caspase inhibitor IDN-6556 ("casp-i"). BC3 cells treated with 20 ng/mL TPA and 10 μM of the pan-caspase inhibitor IDN-6556 ("casp-i") were used as a positive control. IFN-β and IFN- λ1 mRNA levels were measured by RT-qPCR and normalized to 18S rRNA. They are plotted relative to the BC3 positive control. ns = $p>0.05$, ** = $p<0.01$, *** = $p<0.001$, **** = $p<0.0001$. One-Way ANOVA followed by Dunnett's (C, F, G, I, J) or Tukey's (D, E, H) post hoc multiple comparisons test. $n \geq 4$ for all experiments.

Figure 2. The IFN-β reporter allows isolation of cells expressing high and low levels of IFN-β when paracrine signaling is blocked. BC3-IFN-βp-tdTomato reporter cells were treated with 20 ng/mL TPA for 48 hours to induce the lytic cycle ("lytic (+TPA)"). Where indicated, the cells were also treated with 10 μM of the pan-caspase inhibitor IDN-6556 ("casp-i") and a cocktail of antibodies against type I IFNs and their receptor ("anti-IFN Abs") at 1:2000 dilution. **A-C, E-F.** IFN-β, tdTomato, and ORF50 mRNA levels were measured by RT-qPCR and normalized to 18S rRNA. For **A-C** and **F**, mRNA levels are plotted relative to the lytic+casp-i sample. For **E**, mRNA levels are plotted relative to the lytic sample. **D.** Cells were stained for KSHV ORF45 and analyzed by flow cytometry. ns = $p>0.05$, ** = $p<0.01$, *** = $p<0.001$, **** = $p<0.0001$. One-Way ANOVA followed by Dunnett's (A, D, E) or Tukey's (B, C, F) post hoc multiple comparisons test. $n \geq 4$ for all experiments.

Figure 3. IFN-λ1 and IFN-β are coordinately induced in a subset of cells, pointing to heterogeneity in the induction pathway rather than stochastic noise in expression. A. Diagram of coordinate induction of IFN-β and IFN-λ. In "first responder" cells, IFN-β and IFN-λ are induced in response to infection or lytic reactivation downstream of PRRs. In "secondary responder" cells, ISGs such as MxA and many components of the IFN induction pathway like IRF7 are induced in response to signaling downstream of IFN receptors. Induction of genes like IRF7 potentiates IFN induction in these cells. Anti-IFN antibodies block paracrine signaling from IFN-β to prevent ISG induction and potentiation of IFN induction in secondary responder cells. **B-I.** BC3-IFN-

βp-tdTomato reporter cells were treated with 20 ng/ml TPA for 48 hours to induce the lytic cycle ("lytic (+TPA)"). Where indicated, the cells were also treated with 10 μM of the pan-caspase inhibitor IDN-6556 ("casp-i") and/or a cocktail of antibodies against type I IFNs and their receptor ("anti-IFN Abs") at 1:2000 dilution. IFN-λ1 (**B-E**) and MxA (**F-I**) mRNA levels were measured by RT-qPCR and normalized to 18S rRNA. In **B**-**D**, and **F-H,** IFN-λ1 and MxA mRNA levels are plotted relative to the lytic+casp-i sample. In **E** and **I,** IFN-λ1 and MxA mRNA levels are plotted relative to the lytic+casp-i+anti-IFN Abs sample. The lytic+casp-i (**C, G**) or the lytic+casp-i+anti-IFN Abs (**E, I**) samples were sorted based on tdTomato expression and the fold enrichment in IFN-λ1 (**C, E**) and MxA (**G, I**) mRNA levels compared to unsorted ("bulk") samples are plotted in $\log_2$ scale. Results in this figure were obtained from the same samples used in Fig. 1 and are thus directly comparable to IFN-β enrichment shown in that Figure. ns = $p>0.05$, * = $p<0.05$, ** = $p<0.01$, **** = $p<0.0001$, One-Way ANOVA followed by Dunnett's (B, D, F, H) or Tukey's (C, E, G, I) post hoc multiple comparisons test. $n \geq 4$ for all experiments.

Figure 4. TBK1 and IRF3 are necessary but not sufficient to direct IFN-β expression, as they are activated even in cells with low IFN-β expression. BC3-IFN-βp-tdTomato reporter cells were treated with 20 ng/ml TPA for 48 hours to induce the lytic cycle ("lytic (+TPA)"). Where indicated, the cells were also treated with 10 μM of the pan-caspase inhibitor IDN-6556 ("casp-i"), 10 μM of the TBK1 inhibitor MRT76307 ("TBK1i"), 10 μM of the cGAS inhibitor G140 ("cGASi"), and/or a cocktail of antibodies against type I IFNs and their receptor ("anti-IFN Abs") at 1:2000 dilution. **A-B.** IFN-β and IFN-λ1 mRNA levels were measured by qRT-PCR and normalized to 18S rRNA. The

expression levels are plotted relative to “untreated” lytic+casp-i samples that did not receive TBK1i or cGASi treatment for each experiment. n=3. **** = p<0.0001. Two-Way ANOVA followed by Tukey’s post hoc multiple comparisons test. **B-H.** Protein lysates were probed for phosphorylated IRF3 (Ser386), total IRF3, phosphorylated TBK1 (Ser172), total TBK1, and β-actin as a loading control. As a positive control for IRF3 and TBK1 activation/phosphorylation, A549 cells were treated with poly(I:C) for 6 and 48 hours before protein lysates were collected. Protein was isolated from treated BC3-IFN-βp-tdTomato reporter cells without sorting (“bulk”), or after sorting the lytic+casp-i (**C-E**) or lytic+casp-i+anti-IFN Abs (**F-H**) sample based on tdTomato expression (**D-E, G-H)**. Western blot for phosphorylated TBK1 and phosphorylated IRF3 for bulk lytic+casp-i or lytic+casp-i+anti-IFN Abs treated samples and sorted tdTomato+ and tdTomato- samples were quantified by normalizing the density of phosphorylated protein to unphosphorylated protein bands. Phosphorylation levels are plotted relative to the bulk lytic+casp-i or lytic+casp-i+anti-IFN Abs treated samples. **I.** KSHV-negative BJAB cells were treated with vehicle, 20 ng/ml TPA, and/or 10 μM of the pan-caspase inhibitor IDN-6556 (“casp-i”) for 48 hours. Protein was isolated and stained for phosphorylated TBK1, total TBK1, phosphorylated IRF3, and total IRF3. Images shown are representative of 3 replicates (**A-H**) or 2 replicates (**I**).

Figure 5. Levels of the AP-1 subunit ATF2 and phosphorylation of the NF-κB subunit RelA are higher in cells with high IFN-β expression. A. Diagram of the IFN-β enhanceosome and its position on the IFN-β promoter. In the IFN-β enhanceosome, NF-κB is composed of subunits NFKB1 (p50) and RelA, and AP-1 is composed of

subunits ATF2 and c-Jun. **B-C.** Re-analysis of single-cell RNA sequencing (scRNA-seq) data in Tabtieng, Lent, et al 2022. iSLK.219 cells were treated with 1 µg/mL doxycycline for 4 days to induce the lytic cycle ("lytic"). The cells were also treated with 10 µM of the pan-caspase inhibitor IDN-6556 ("casp-i"), as well as a mixture of antibodies against type I IFNs and its receptor ("anti-IFN Abs") (**C** only) to block IFN-β paracrine signaling. The average mRNA levels of genes in the IFN-β enhanceosome from the scRNA-seq data are shown for each of the 12 clusters of cells identified by the original analysis (indicated by different colors above the heatmap). Clusters were classified as "latent". "lytic", or "lytic IFN-β-positive" based on the pattern of viral genes they expressed and whether they also expressed IFN-β. The "lytic IFN-β-positive" clusters were further separated into two groups based on the IFN-β status of individual cells. **D-F, I-J.** BC3-IFN-βp-tdTomato reporter cells were treated with 20 ng/ml TPA for 48 hours to induce the lytic cycle ("lytic (+TPA)"), 10 µM of the pan-caspase inhibitor IDN-6556 ("casp-i"), and/or a cocktail of antibodies against type I IFNs and their receptor ("anti-IFN Abs") to block IFN-β paracrine signaling. Protein was isolated from BC3-IFN-βp-tdTomato reporter cells without sorting ("bulk"), or after sorting the lytic+casp-i+anti-IFN Abs based on tdTomato expression. Western blots were probed for ATF2 (**D**), c-Jun (**D**), or total RelA and phosphorylated RelA (Ser536) (**I**) and β-actin as a loading control. Levels of ATF2 (**E**) and c-Jun (**F**) in sorted samples were quantified from the western blots, normalized to β-actin, and plotted relative to bulk lytic+casp-i+ anti-IFN Abs samples. Levels of phosphorylated RelA (Ser536) (**J**) were quantified by normalizing to total RelA and plotted relative to bulk lytic+casp-i+ anti-IFN Abs samples. **G, H, K.** KSHV-negative BJAB cells were treated with vehicle, 20 ng/ml TPA and/or 10 µM of the pan-caspase

inhibitor IDN-6556 (“casp-i”) for 48 hrs. Protein was isolated and stained for ATF2 (**G**), c-Jun (**H**), phosphorylated (Ser536) and total RelA (**K**), and β-actin as a loading control. Images are representative of 4 replicates (**D**), 3 replicates (**I**), or 2 replicates (**G, H, K**). ns = $p>0.05$, * = $p<0.05$, ** = $p<0.01$, One-Way ANOVA followed by Tukey’s post hoc multiple comparisons test.

Figure 6. Model of regulation of heterogeneous IFN-β expression by components of the IFN-β enhanceosome. *(Left)* In the rare cells that induce IFN-β during viral infection as “first responders”, there are high levels of the AP-1 factor ATF2 and both the NF-κB subunit RelA and IRF3 become phosphorylated in response to infection. This results in the formation of the IFN-β enhanceosome and IFN-β and IFN-λ1 transcription. *(Right)* In the majority of virally infected cells, there are lower amounts of ATF2, and RelA is not phosphorylated during infection. While IRF3 is still activated, the full IFN-β enhanceosome does not form and IFN-β and IFN-λ1 are not induced.

Figure 1

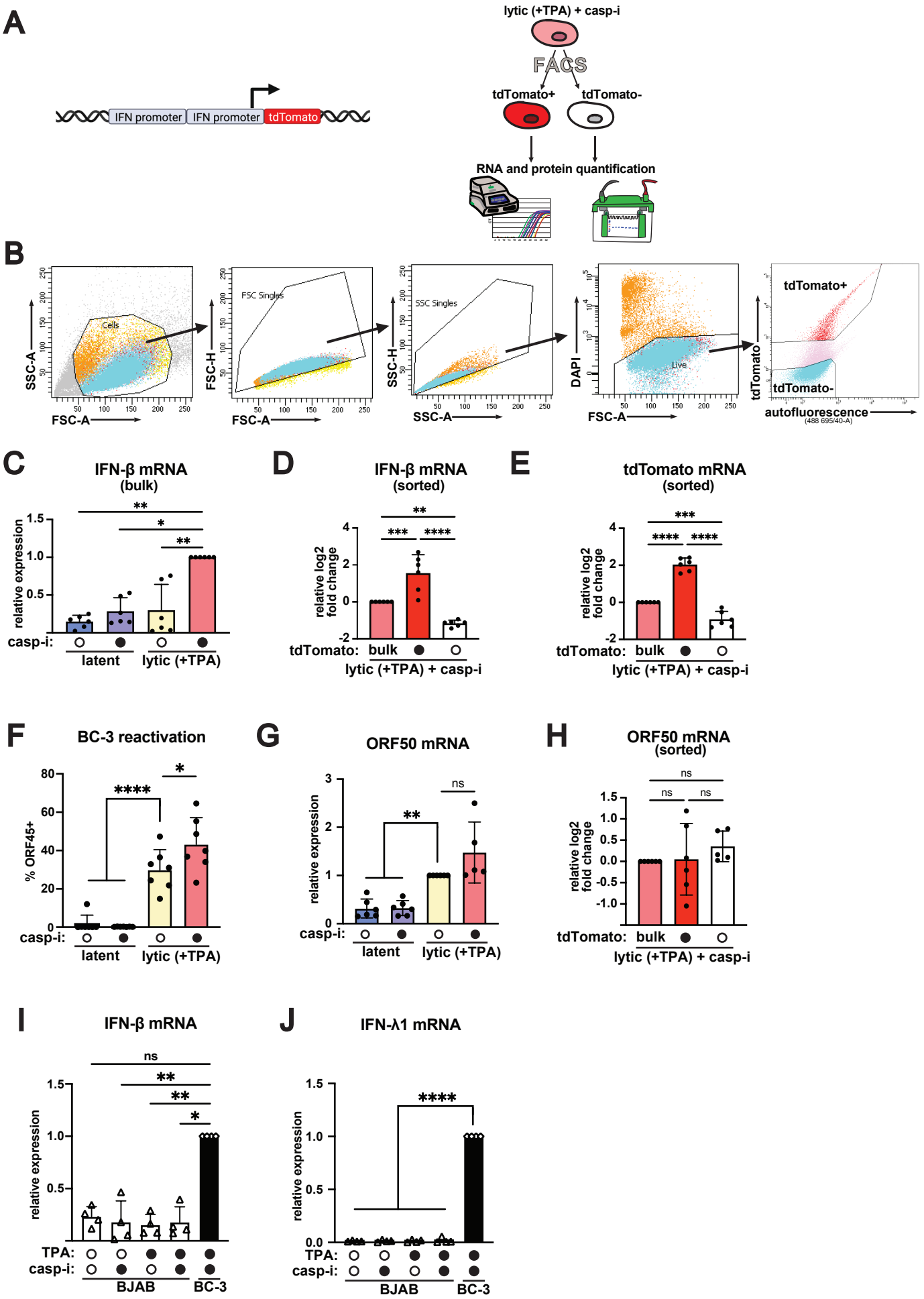
A
IFN promoter
IFN promoter
tdTomato
lytic (+TPA) + casp-i
FACS
tdTomato+
tdTomato-
RNA and protein quantification
B
Cells
SSC-A
FSC-A
FSC Singles
FSC-H
FSC-A
SSC Singles
SSC-H
SSC-A
Live
DAPI
FSC-A
tdTomato+
tdTomato-
tdTomato
autofluorescence
(488 695/40-A)
C
IFN-β mRNA
(bulk)
relative expression
casp-i:
latent
lytic (+TPA)
D
IFN-β mRNA
(sorted)
relative log2 fold change
tdTomato:
bulk
lytic (+TPA) + casp-i
E
tdTomato mRNA
(sorted)
relative log2 fold change
tdTomato:
bulk
lytic (+TPA) + casp-i
F
BC-3 reactivation
% ORF45+
casp-i:
latent
lytic (+TPA)
G
ORF50 mRNA
relative expression
casp-i:
latent
lytic (+TPA)
H
ORF50 mRNA
(sorted)
relative log2 fold change
tdTomato:
bulk
lytic (+TPA) + casp-i
I
IFN-β mRNA
relative expression
TPA:
casp-i:
BJAB
BC-3
J
IFN-λ1 mRNA
relative expression
TPA:
casp-i:
BJAB
BC-3

Figure 1. An IFN-β-promoter driven fluorescent reporter allows isolation of cells expressing high and low levels of IFN-β. A. Diagram of the IFN-βp-tdTomato reporter and sorting strategy. Two copies of the 303 bp minimal promoter sequence for the human IFNB1 gene were cloned in front of the tdTomato fluorophore. This cassette was then introduced in BC-3 cells via lentiviral transduction for stable integration. Cells were sorted based on tdTomato expression and RNA and protein samples were collected from the same experiment. **B-H.** BC3-IFN-βp-tdTomato reporter cells were treated with 20 ng/mL TPA for 48 hours to induce the lytic cycle ("lytic (+TPA)"). Where indicated, the cells were also treated with 10 μM of the pan-caspase inhibitor IDN-6556 ("casp-i"). **B.** Gating strategy for FACS. **C-E**, **G-H**. IFN-β, tdTomato, and ORF50 mRNA levels were measured by RT-qPCR and normalized to 18S rRNA. For **C-E** and **H**, mRNA levels are plotted relative to the lytic+casp-i sample. For **G**, mRNA levels are plotted relative to the lytic sample. **H.** Cells were stained for KSHV ORF45 and analyzed by flow cytometry. **I-J.** KSHV-negative BJAB cells were treated with 20 ng/mL TPA for 48 hours. Where indicated, the cells were also treated with 10 μM of the pan-caspase inhibitor IDN-6556 ("casp-i"). BC3 cells treated with 20 ng/mL TPA and 10 μM of the pan-caspase inhibitor IDN-6556 ("casp-i") were used as a positive control. IFN-β and IFN- λ1 mRNA levels were measured by RT-qPCR and normalized to 18S rRNA. They are plotted relative to the BC3 positive control. ns = $p>0.05$, ** = $p<0.01$, *** = $p<0.001$, **** = $p<0.0001$. One-Way ANOVA followed by Dunnett's (C, F, G, I, J) or Tukey's (D, E, H) post hoc multiple comparisons test. $n \geq 4$ for all experiments.

Figure 2

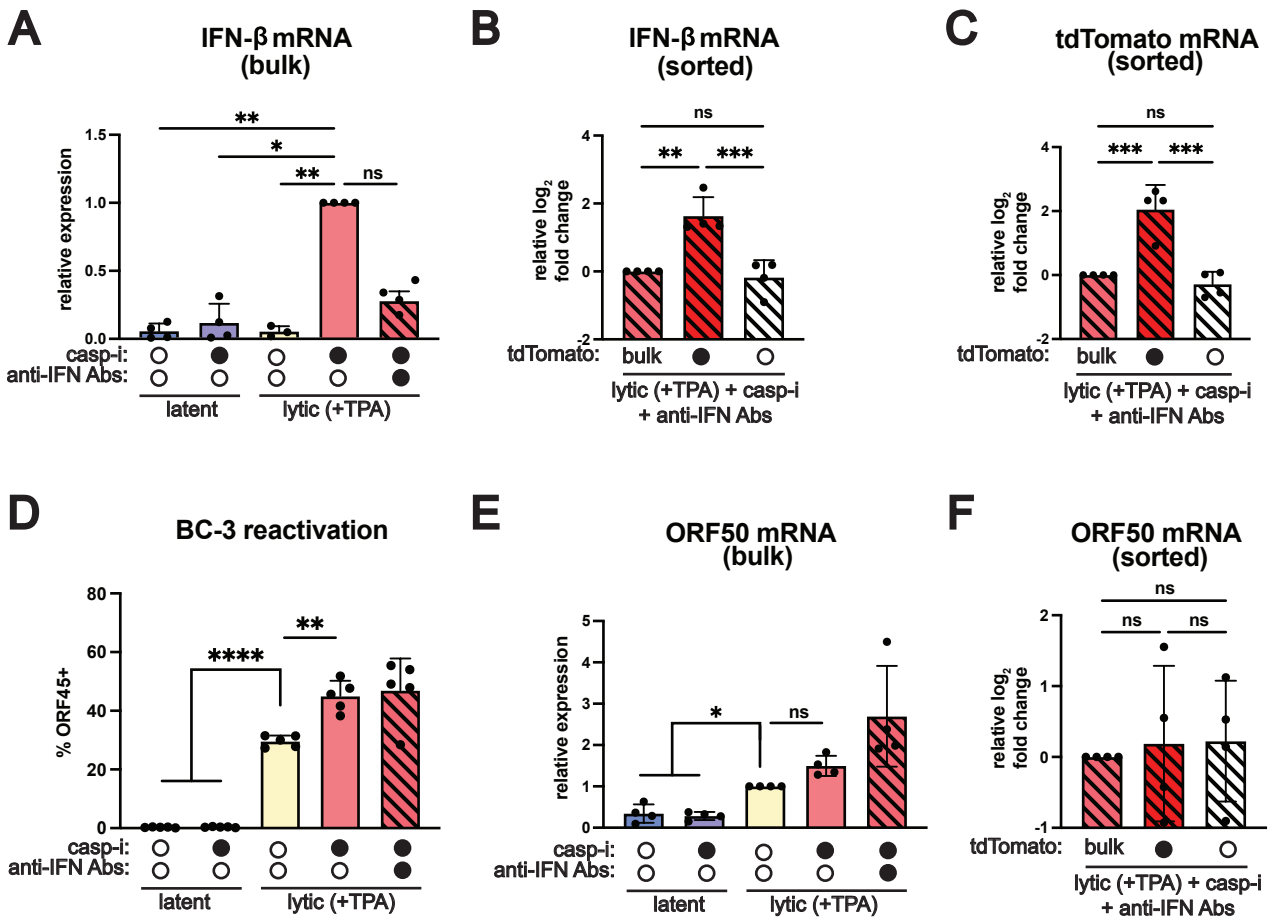

Figure 2. The IFN-β reporter allows isolation of cells expressing high and low levels of IFN-β when paracrine signaling is blocked. BC3-IFN-βp-tdTomato reporter cells were treated with 20 ng/mL TPA for 48 hours to induce the lytic cycle ("lytic (+TPA)"). Where indicated, the cells were also treated with 10 μM of the pan-caspase inhibitor IDN-6556 ("casp-i") and a cocktail of antibodies against type I IFNs and their receptor ("anti-IFN Abs") at 1:2000 dilution. **A-C**, **E-F**. IFN-β, tdTomato, and ORF50 mRNA levels were measured by RT-qPCR and normalized to 18S rRNA. For **A-C** and **F**, mRNA levels are plotted relative to the lytic+casp-i sample. For **E**, mRNA levels are plotted relative to the lytic sample. **D.** Cells were stained for KSHV ORF45 and analyzed by flow cytometry. ns = p>0.05, ** = p<0.01, *** = p<0.001, **** = p<0.0001. One-Way ANOVA followed by Dunnett's (A, D, E) or Tukey's (B, C, F) post hoc multiple comparisons test. n≥ 4 for all experiments.

Figure 3

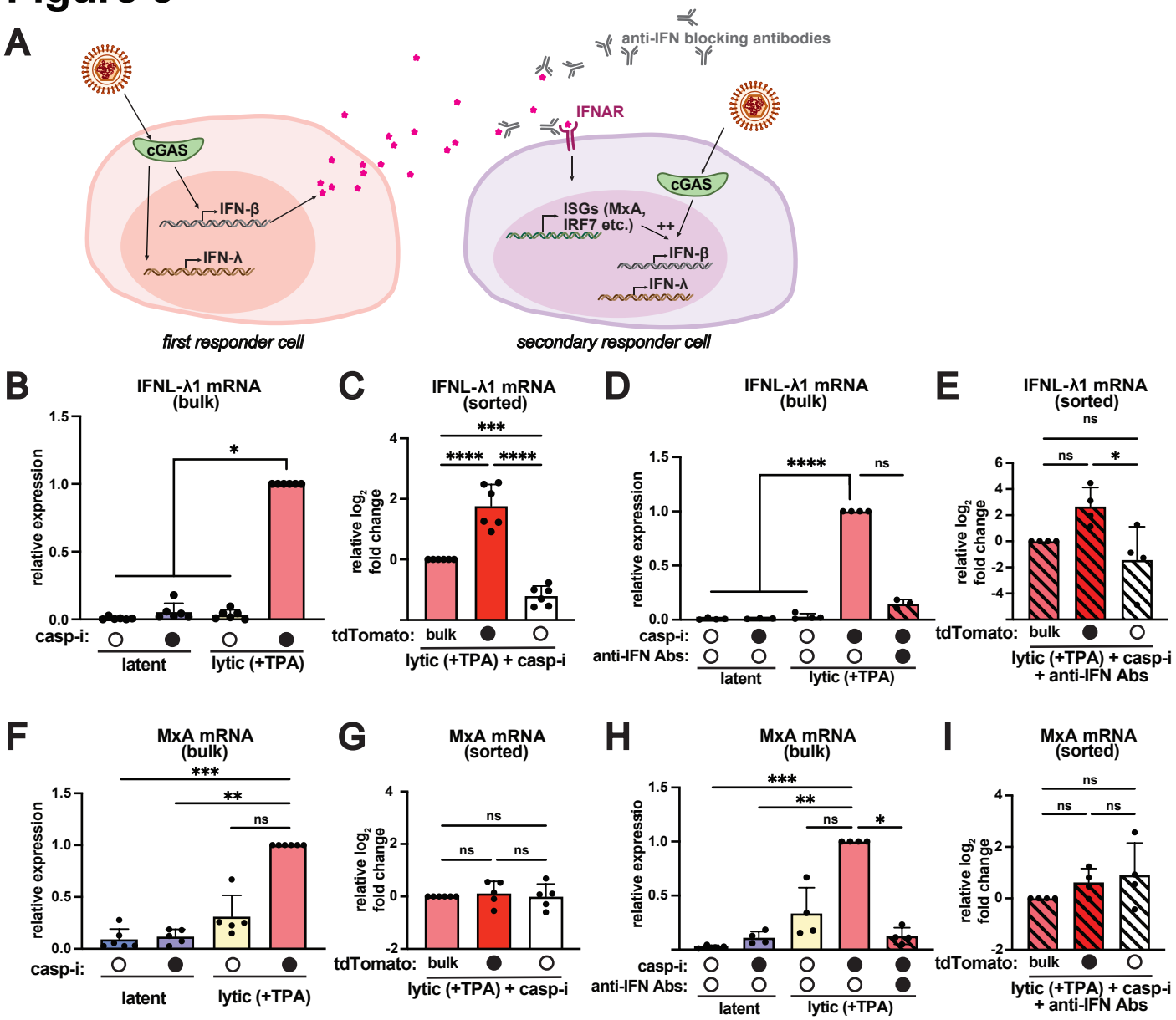

Figure 3. IFN-λ1 and IFN-β are coordinately induced in a subset of cells, pointing to heterogeneity in the induction pathway rather than stochastic noise in expression. A. Diagram of coordinate induction of IFN-β and IFN-λ. In "first responder" cells, IFN-β and IFN-λ are induced in response to infection or lytic reactivation downstream of PRRs. In "secondary responder" cells, ISGs such as MxA and many components of the IFN induction pathway like IRF7 are induced in response to signaling downstream of IFN receptors. Induction of genes like IRF7 potentiates IFN induction in these cells. Anti-IFN antibodies block paracrine signaling from IFN-β to prevent ISG induction and potentiation of IFN induction in secondary responder cells. **B-I.** BC3-IFN-βp-tdTomato reporter cells were treated with 20 ng/ml TPA for 48 hours to induce the lytic cycle ("lytic (+TPA)"). Where indicated, the cells were also treated with 10 μM of the pan-caspase inhibitor IDN-6556 ("casp-i") and/or a cocktail of antibodies against type I IFNs and their receptor ("anti-IFN Abs") at 1:2000 dilution. IFN-λ1 (**B-E**) and MxA (**F-I**) mRNA levels were measured by RT-qPCR and normalized to 18S rRNA. In **B-D**, and **F-H**, IFN-λ1 and MxA mRNA levels are plotted relative to the lytic+casp-i sample. In **E** and **I**, IFN-λ1 and MxA mRNA levels are plotted relative to the lytic+casp-i+anti-IFN Abs sample. The lytic+casp-i (**C, G**) or the lytic+casp-i+anti-IFN Abs (**E, I**) samples were sorted based on tdTomato expression and the fold enrichment in IFN-λ1 (**C, E**) and MxA (**G, I**) mRNA levels compared to unsorted ("bulk") samples are plotted in log2 scale. Results in this figure were obtained from the same samples used in Fig. 1 and are thus directly comparable to IFN-β enrichment shown in that Figure. ns = p>0.05, * = p<0.05, ** = p<0.01, **** = p<0.0001, One-Way ANOVA followed by Dunnett's (B, D, F, H) or Tukey's (C, E, G, I) post hoc multiple comparisons test. n≥ 4 for all experiments.

Figure 4

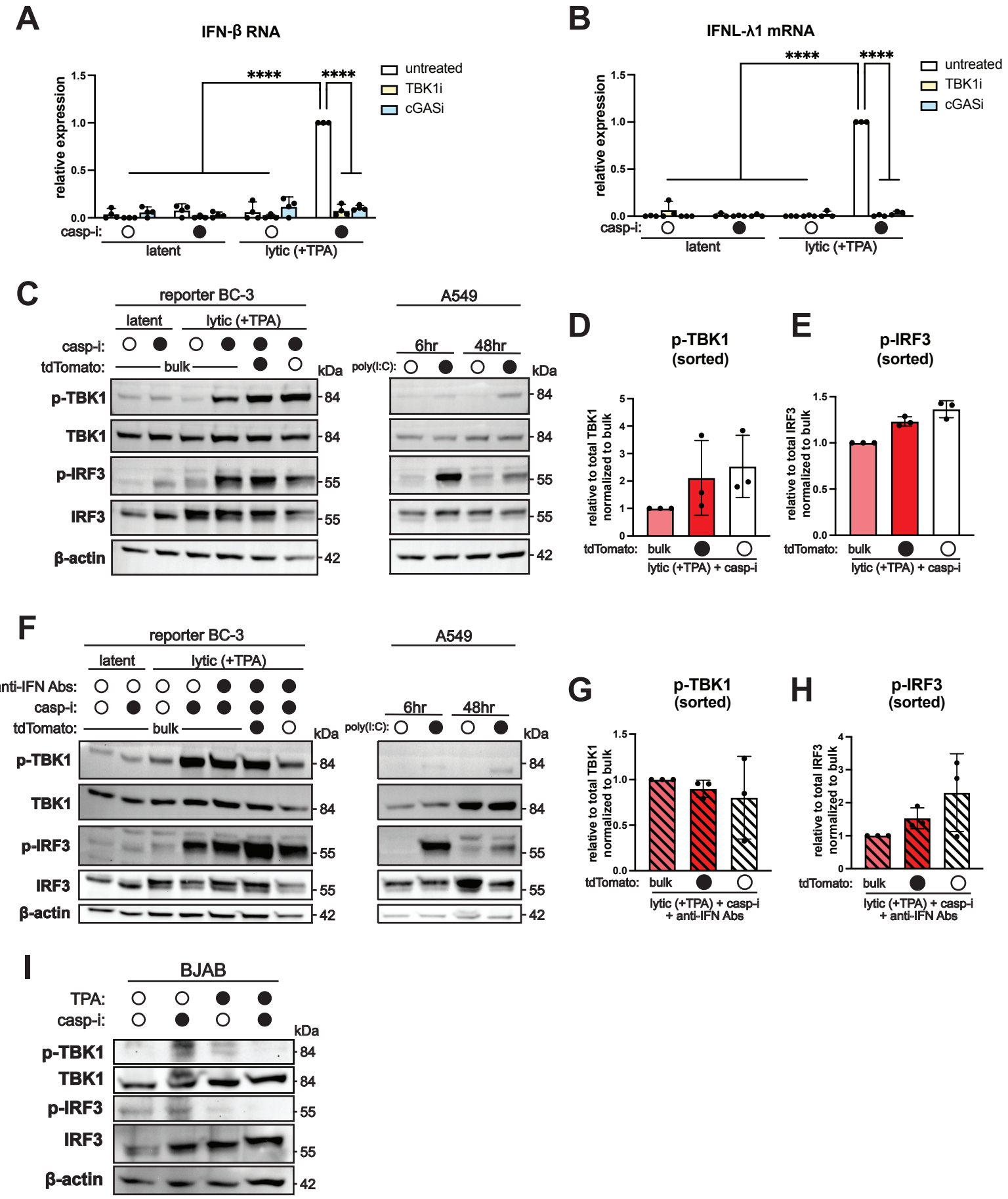
A
IFN-β RNA
relative expression
1.5
1.0
0.5
0.0
****
****
untreated
TBK1i
cGASi
casp-i:
latent
lytic (+TPA)
B
IFNL-λ1 mRNA
relative expression
****
****
untreated
TBK1i
cGASi
casp-i:
latent
lytic (+TPA)
C
reporter BC-3
latent
lytic (+TPA)
casp-i:
tdTomato:
bulk
kDa
p-TBK1
TBK1
p-IRF3
IRF3
β-actin
84
84
55
55
42
A549
6hr
48hr
poly(I:C):
kDa
84
84
55
55
42
D
p-TBK1
(sorted)
relative to total TBK1
normalized to bulk
tdTomato:
bulk
lytic (+TPA) + casp-i
E
p-IRF3
(sorted)
relative to total IRF3
normalized to bulk
tdTomato:
bulk
lytic (+TPA) + casp-i
F
reporter BC-3
latent
lytic (+TPA)
anti-IFN Abs:
casp-i:
tdTomato:
bulk
kDa
p-TBK1
TBK1
p-IRF3
IRF3
β-actin
84
84
55
55
42
A549
6hr
48hr
poly(I:C):
kDa
84
84
55
55
42
G
p-TBK1
(sorted)
relative to total TBK1
normalized to bulk
tdTomato:
bulk
lytic (+TPA) + casp-i
+ anti-IFN Abs
H
p-IRF3
(sorted)
relative to total IRF3
normalized to bulk
tdTomato:
bulk
lytic (+TPA) + casp-i
+ anti-IFN Abs
I
BJAB
TPA:
casp-i:
kDa
p-TBK1
TBK1
p-IRF3
IRF3
β-actin
84
84
55
55
42

Figure 4. TBK1 and IRF3 are necessary but not sufficient to direct IFN-β expression, as they are activated even in cells with low IFN-β expression. BC3-IFN-βp-tdTomato reporter cells were treated with 20 ng/ml TPA for 48 hours to induce the lytic cycle ("lytic (+TPA)"). Where indicated, the cells were also treated with 10 μM of the pan-caspase inhibitor IDN-6556 ("casp-i"), 10 μM of the TBK1 inhibitor MRT76307 ("TBK1i"), 10 μM of the cGAS inhibitor G140 ("cGASi"), and/or a cocktail of antibodies against type I IFNs and their receptor ("anti-IFN Abs") at 1:2000 dilution. **A-B.** IFN-β and IFN-λ1 mRNA levels were measured by qRT-PCR and normalized to 18S rRNA. The expression levels are plotted relative to "untreated" lytic+casp-i samples that did not receive TBK1i or cGASi treatment for each experiment. n=3. **** = $p<0.0001$. Two-Way ANOVA followed by Tukey's post hoc multiple comparisons test. **B-H.** Protein lysates were probed for phosphorylated IRF3 (Ser386), total IRF3, phosphorylated TBK1 (Ser172), total TBK1, and β-actin as a loading control. As a positive control for IRF3 and TBK1 activation/phosphorylation, A549 cells were treated with poly(I:C) for 6 and 48 hours before protein lysates were collected. Protein was isolated from treated BC3-IFN-βp-tdTomato reporter cells without sorting ("bulk"), or after sorting the lytic+casp-i (**C-E**) or lytic+casp-i+anti-IFN Abs (**F-H**) sample based on tdTomato expression (**D-E**, **G-H**). Western blot for phosphorylated TBK1 and phosphorylated IRF3 for bulk lytic+casp-i or lytic+casp-i+anti-IFN Abs treated samples and sorted tdTomato+ and tdTomato- samples were quantified by normalizing the density of phosphorylated protein to unphosphorylated protein bands. Phosphorylation levels are plotted relative to the bulk lytic+casp-i or lytic+casp-i+anti-IFN Abs treated samples. I. KSHV-negative BJAB cells were treated with vehicle, 20 ng/ml TPA, and/or 10 μM of the pan-caspase inhibitor IDN-6556 ("casp-i") for 48 hours. Protein was isolated and stained for phosphorylated TBK1, total TBK1, phosphorylated IRF3, and total IRF3. Images shown are representative of 3 replicates (A-H) or 2 replicates (I).

Figure 5

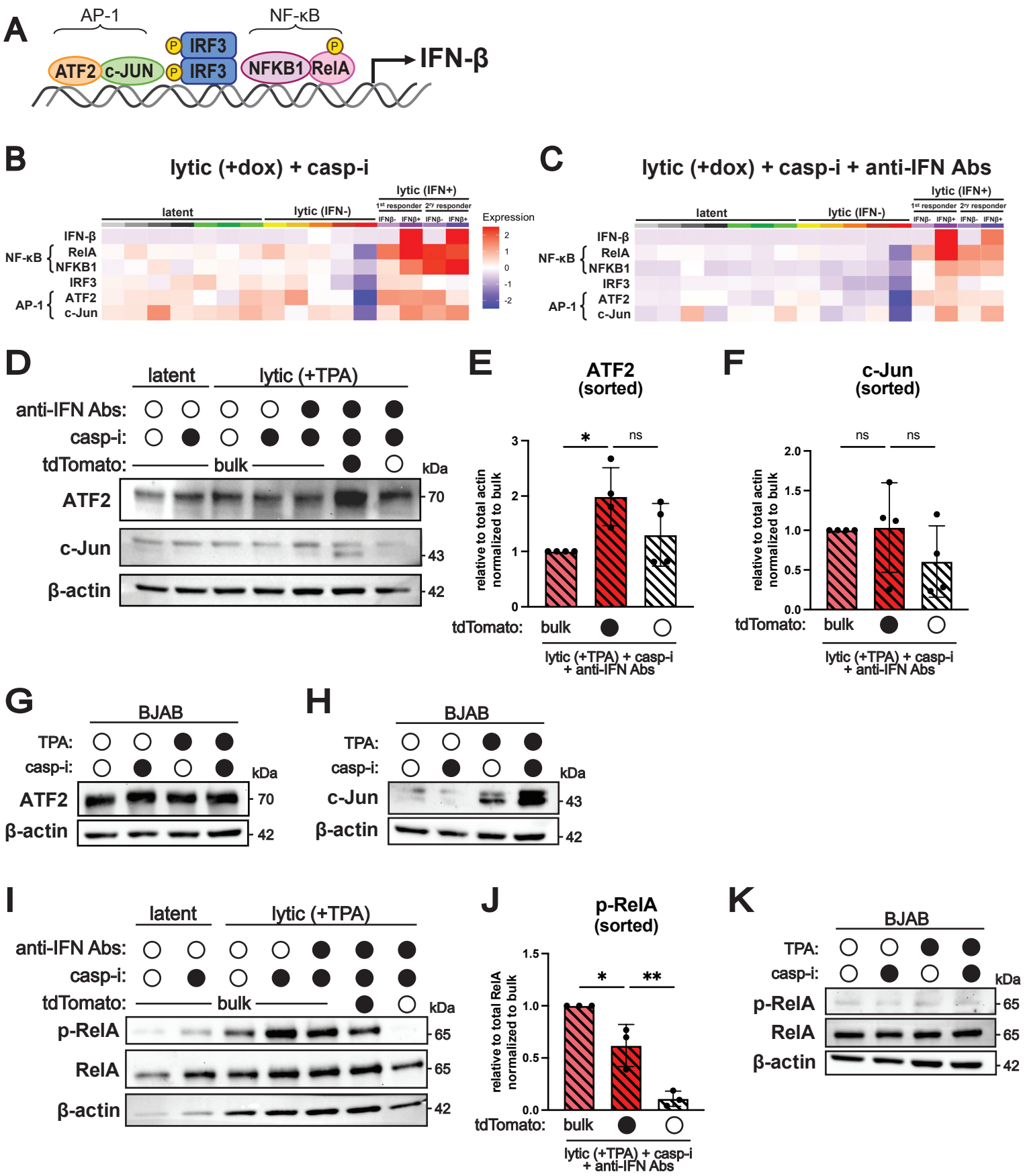
A
AP-1
NF-κB
IRF3
IRF3
ATF2
c-JUN
NFKB1
RelA
IFN-β
B
lytic (+dox) + casp-i
latent
lytic (IFN-)
lytic (IFN+)
1st responder
2ry responder
IFNβ-
IFNβ+
Expression
IFN-β
NF-κB
RelA
NFKB1
IRF3
AP-1
ATF2
c-Jun
C
lytic (+dox) + casp-i + anti-IFN Abs
D
latent
lytic (+TPA)
anti-IFN Abs:
casp-i:
tdTomato:
bulk
kDa
ATF2
c-Jun
β-actin
70
43
42
E
ATF2
(sorted)
relative to total actin normalized to bulk
*
ns
tdTomato:
bulk
lytic (+TPA) + casp-i
+ anti-IFN Abs
F
c-Jun
(sorted)
ns
ns
G
BJAB
TPA:
casp-i:
H
I
p-RelA
RelA
65
J
p-RelA
(sorted)
relative to total RelA normalized to bulk
**
K

Figure 5. Levels of the AP-1 subunit ATF2 and phosphorylation of the NF-κB subunit RelA are higher in cells with high IFN-β expression. A. Diagram of the IFN-β enhanceosome and its position on the IFN-β promoter. In the IFN-β enhanceosome, NF-κB is composed of subunits NFKB1 (p50) and RelA, and AP-1 is composed of subunits ATF2 and c-Jun. **B-C.** Re-analysis of single-cell RNA sequencing (scRNA-seq) data in Tabtieng, Lent, et al 2022. iSLK.219 cells were treated with 1 μg/mL doxycycline for 4 days to induce the lytic cycle ("lytic"). The cells were also treated with 10 μM of the pan-caspase inhibitor IDN-6556 ("casp-i"), as well as a mixture of antibodies against type I IFNs and its receptor ("anti-IFN Abs") (**C** only) to block IFN-β paracrine signaling. The average mRNA levels of genes in the IFN-β enhanceosome from the scRNA-seq data are shown for each of the 12 clusters of cells identified by the original analysis (indicated by different colors above the heatmap). Clusters were classified as "latent", "lytic", or "lytic IFN-β-positive" based on the pattern of viral genes they expressed and whether they also expressed IFN-β. The "lytic IFN-β-positive" clusters were further separated into two groups based on the IFN-β status of individual cells. **D-F**, **I-J**. BC3-IFN-βp-tdTomato reporter cells were treated with 20 ng/ml TPA for 48 hours to induce the lytic cycle ("lytic (+TPA)"), 10 μM of the pan-caspase inhibitor IDN-6556 ("casp-i"), and/or a cocktail of antibodies against type I IFNs and their receptor ("anti-IFN Abs") to block IFN-β paracrine signaling. Protein was isolated from BC3-IFN-βp-tdTomato reporter cells without sorting ("bulk"), or after sorting the lytic+casp-i+anti-IFN Abs based on tdTomato expression. Western blots were probed for ATF2 (**D**), c-Jun (**D**), or total RelA and phosphorylated RelA (Ser536) (**I**) and β-actin as a loading control. Levels of ATF2 (**E**) and c-Jun (**F**) in sorted samples were quantified from the western blots, normalized to β-actin, and plotted relative to bulk lytic+casp-i+ anti-IFN Abs samples. Levels of phosphorylated RelA (Ser536) (**J**) were quantified by normalizing to total RelA and plotted relative to bulk lytic+casp-i+ anti-IFN Abs samples. **G**, **H**, **K**. KSHV-negative BJAB cells were treated with vehicle, 20 ng/ml TPA and/or 10 μM of the pan-caspase inhibitor IDN-6556 ("casp-i") for 48 hrs. Protein was isolated and stained for ATF2 (**G**), c-Jun (**H**), phosphorylated (Ser536) and total RelA (**K**), and β-actin as a loading control. Images are representative of 4 replicates (D), 3 replicates (I), or 2 replicates (G, H, K). ns = $p>0.05$, * = $p<0.05$, ** = $p<0.01$, One-Way ANOVA followed by Tukey's post hoc multiple comparisons test.

Figure 6

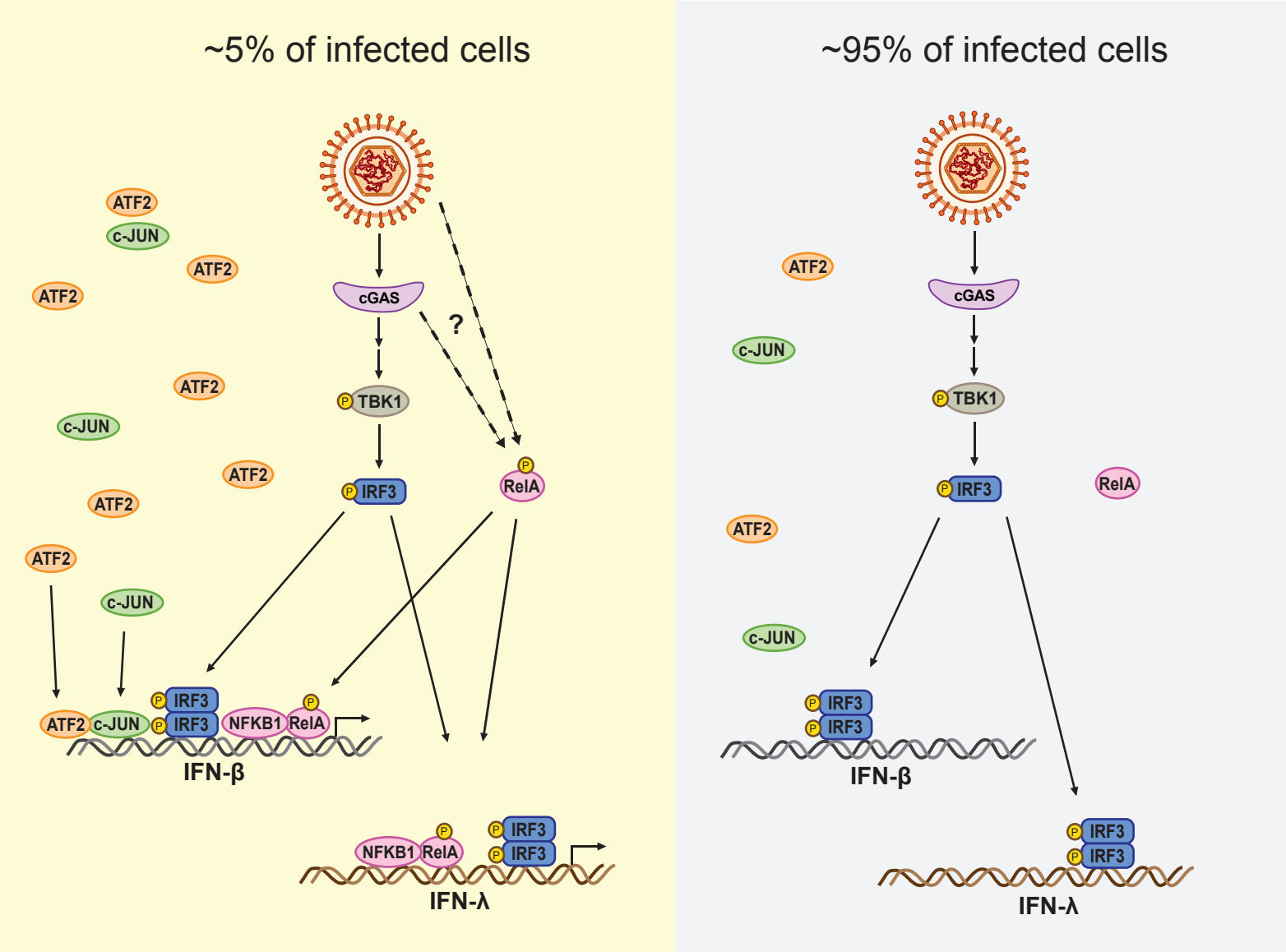

Figure 6. Model of regulation of heterogeneous IFN-β expression by components of the IFN-β enhanceosome. (*Left*) In the rare cells that induce IFN-β during viral infection as "first responders", there are high levels of the AP-1 factor ATF2 and both the NF-κB subunit RelA and IRF3 become phosphorylated in response to infection. This results in the formation of the IFN-β enhanceosome and IFN-β and IFN-λ1 transcription. (*Right*) In the majority of virally infected cells, there are lower amounts of ATF2, and RelA is not phosphorylated during infection. While IRF3 is still activated, the full IFN-β enhanceosome does not form and IFN-β and IFN-λ1 are not induced.